

**PURDUE UNIVERSITY
GRADUATE SCHOOL
Thesis/Dissertation Acceptance**

This is to certify that the thesis/dissertation prepared

By Daniel J. McMahon

Entitled
Investigation of Isotope Effects of Ozone as a Function of Temperature

For the degree of Master of Science

Is approved by the final examining committee:

Dr. Greg Michalski

Dr. Paul Shepson

Dr. Harshvardhan

To the best of my knowledge and as understood by the student in the *Thesis/Dissertation Agreement, Publication Delay, and Certification/Disclaimer (Graduate School Form 32)*, this thesis/dissertation adheres to the provisions of Purdue University's "Policy on Integrity in Research" and the use of copyrighted material.

Dr. Greg Michalski

Approved by Major Professor(s): _____

Approved by: Dr. Indrajeet Chaubey

03/03/2014

Head of the Department Graduate Program

Date

INVESTIGATION OF ISOTOPE EFFECTS OF OZONE AS A FUNCTION OF
TEMPERATURE

A Thesis

Submitted to the Faculty

of

Purdue University

by

Daniel J. McMahon

In Partial Fulfillment of the

Requirements for the Degree

of

Master of Science

May 2014

Purdue University

West Lafayette, Indiana

TABLE OF CONTENTS

	Page
LIST OF TABLES	iv
LIST OF FIGURES	v
ABSTRACT	vii
CHAPTER 1. INTRODUCTION	1
1.1 Ozone in the Troposphere	3
1.2 Stratospheric Ozone	6
1.3 Oxygen Isotopic Variations.....	10
1.4 Mass Independent Fractionation and Enrichment of Ozone	16
1.5 Application of Predicted and Measured Ozone Isotopic Enrichment	19
CHAPTER 2. TEMPERATURE DEPENDENT ENRICHMENT OF OZONE.....	22
2.1 Introduction	22
2.2 Experimental Setup	24
2.3 Results	27
2.4 Discussion	28
2.4.1 O +O ₂ Exchange.....	28
2.4.2 Temperature and Pressure Dependence	31
2.4.3 Mass Independence and Calculation of $\Delta^{17}\text{O}$ and r_{50}	33
2.4.4 Fit Model.....	38
2.4.5 Single IRC Models.....	39
2.4.6 Split Pathway IRC Model	42
2.4.7 Model Isotopic Enrichment Predictions.....	45
2.5 Comparison with Atmospheric Measurements	46
2.5.1 Predicted O ₃ $\Delta^{17}\text{O}$ Enrichment as a Function of Altitude.....	47
2.6 Conclusions and Limitations.....	49

	Page
CHAPTER 3. A PROXY METHOD FOR SAMPLING ISOTOPES OF O ₃	51
3.1 Introduction	51
3.2 O ₃ /NO ₂ ⁻ Reactivity and Isotope Transfer	53
3.3 Ozone Scrubbing Method Using a NO ₂ ⁻ Bubbler	54
3.4 NO ₃ ⁻ Contaminant in NO ₂ ⁻ Bubbler Solutions.....	57
3.5 Eliminating NO ₃ ⁻ Contaminant from the NO ₂ ⁻ Solution.....	58
3.5.1 Eliminating NO ₃ ⁻ Contaminant from the NO ₂ ⁻ Solution by Chromatography	58
3.5.2 Eliminating NO ₃ ⁻ Contaminant from the NO ₂ ⁻ Solution by Cadmium Reduction	60
3.6 Removing Residual NO ₂ ⁻ From Bubbling Solution	63
3.6.1 NO ₂ ⁻ Removal by Reaction with Azide	66
3.6.2 NO ₂ ⁻ Removal with Sulfamic Acid	68
3.7 NO ₃ ⁻ Processing Methods.....	69
3.7.1 Silver NO ₃ ⁻ Thermal Decomposition	69
3.7.2 Bacterial Denitrification.....	71
3.8 Potential Improvements.....	73
3.9 Conclusions and Implications	75
CHAPTER 4. CONCLUSIONS	77
4.1 Future Work	78
4.2 Implications	80
LIST OF REFERENCES	83
APPENDIX	90

LIST OF TABLES

Table	Page
Table 2.1: O ₃ enrichments relative to starting gas composition.....	27
Table 2.2: Enrichment slope as a function of temperature	32
Table 2.3: Photochemical box model reactions and rates.....	41
Table 2.4: Applied IRC values for all isotopically substituted O ₃ formation reactions for this study's models as well as previous works (@300K)	43
Table 2.5: Predicted enrichment and symmetry ratios from Model 3	44
Table 2.6: Model output and deviation from experimental data for isotopic enrichment of O ₃	46
Table 2.7: Average tropospheric O ₃ data and predicted asymmetric enrichment compared with model 3 prediction(Johnston et al., 1997;William C.Vicars et al., 2012).	47

LIST OF FIGURES

Figure	Page
Figure 1.1: NO _x cycle and peroxy radical O ₃ formation(Seinfeld and Pandis, 1998).....	5
Figure 1.2: O ₃ isopleths for varied NO _x /VOC ratios(Jeffries and R Crouse, 1991).....	5
Figure 1.3: O ₃ absorption spectrum(J.Orphal, 2002)	7
Figure 1.4: O ₃ concentration with altitude(Seinfeld and Pandis, 1998).	8
Figure 1.5: O and O ₃ number densities in the stratosphere(Wayne, 1996).....	10
Figure 1.6: Ozone's isotopic forms	12
Figure 1.7: Terrestrial Fractionation Line(TFL) and other characterized atmospheric species(Krystin Riha, 2013).....	16
Figure 2.1: O ₃ formation and collection apparatus	24
Figure 2.2: Pen-Ray mercury lamp emission spectra (UVP, 2014).....	25
Figure 2.3 Pressure corrected O ₃ enrichment (triangles) measured relative to the starting gas represents all reactions in the chapman mechanism including a depletion associated with O+O ₂ exchange (squares).....	30
Figure 2.4: Comparison between experimental enrichments of this study (triangles), Morton (1990) (squares) and Janssen (2002) (circles). All data has been pressure corrected and O+O ₂ depletion subtracted for direct comparison of enrichment associated with the recombination reaction.....	30

Figure	Page
Figure 2.5: λ determination from the slope of the O+O ₂ enrichment partition function calculation.	35
Figure 2.6: $\Delta^{17}\text{O}$ variation caused by different equation use. Adapted from Miller, 2002	35
Figure 2.7: Predicted $\Delta^{17}\text{O}_a$ change with altitude(troposphere).	48
Figure 2.8: Predicted $\Delta^{17}\text{O}_a$ change with altitude (stratosphere).	49
Figure 3.1: Laboratory O ₃ bubbler apparatus	54
Figure 3.2: O ₃ scrubbing efficiency with NO ₂ - concentration	55
Figure 3.3: CuCd granules produced from both methods(Cortas et al., 1990)	62
Figure 3.4: $\Delta^{17}\text{O}$ measured from Hoffman NO ₃ ⁻ isolated from a NO ₂ ⁻ solution.	65
Figure 3.5: Blank increase when baseline blank is considered the amount present in the solution with the smallest NO ₃ ⁻ added.	65

ABSTRACT

McMahon, Daniel J. M.S., Purdue University, May 2014. Investigation of Isotope Effects of Ozone as a Function of Temperature. Major Professor: Dr. Greg Michalski.

Ozone is an important oxidizer in the atmosphere and plays a crucial role as a cleanser, removing various compounds such NO_x and SO_x . It also is intriguing to those that study stable isotopes as it has a unique signature found in no other oxygen containing molecule. Ozone is observed to fractionate mass independently, which means it does not follow the typical $\delta^{17}\text{O} / \delta^{18}\text{O} = 0.52$ ratio expected for molecules enriched with ^{17}O and ^{18}O . The magnitude of ozone's mass independent enrichment has been studied in laboratory experiments and atmospheric observations but its explanation is still incomplete. Symmetry of the isotopically substituted ozone is postulated to be the source of mass independent enrichment and this thesis will build on that explanation to examine the magnitude of isotopic enrichment as a function of temperature.

Understanding of the kinetics of ozone formation has come a long way from early predictions of enrichments $>200\%$. However, while our ability to accurately model ozone's bulk isotopic enrichment has improved to include separate rates for the formation of asymmetric and symmetric ozone, rate experiments are sparse for ^{17}O and of low precision. To improve our understanding of ozone's enrichment, this study presents a temperature dependent enrichment experiment and series of models to predict

asymmetric mass independent fractionation. This also served to examine ozone's enrichment in the troposphere by using an open flow experimental setup which is in contrast to previous works examining ozone enrichment in a closed system. Our experimental observations show that under tropospheric conditions, ozone should have $\delta^{17}\text{O} \approx 75\text{‰}$, $\delta^{18}\text{O} \approx 80\text{‰}$, and $\Delta^{17}\text{O} \approx 33$. The models were able to match experimental values, often within 1‰, and with minimal assumptions, predict asymmetric ozone to have $\Delta^{17}\text{O}=47.5\text{‰}$. This value is important as ozone transfers its terminal atom to species it oxidizes and will be the starting point to using ozone as a tracer in atmospheric reactions.

Modeling improves our understanding of ozone's enrichments but these predictions must be validated by atmospheric observations. Previous tropospheric ozone sampling studies produced data of low precision but still showed relatively good agreement with our laboratory observations. In order to obtain better isotopic data a proxy method for sampling ozone's terminal atom is needed. Reaction with nitrite in solution is promising as the reaction is rapid and efficient. However we were unable to obtain tropospheric ozone observations as nitrite processing methods could not be perfected to remove nitrate blank concentrations. We do present the merits of using nitrite to react with atmospheric ozone and the suggest purification steps that may allow this method to be successful in the future

CHAPTER 1. INTRODUCTION

This thesis is an examination of isotope effects arising during ozone formation. While ozone's function in the atmosphere is of great importance, understanding its isotopic variations through its own cyclical formation and destruction is limited despite being exceptionally useful to allow for tracing of the subsequent reactions it is involved with.

Ozone (O_3) is an essential component of the atmosphere that is both beneficial and harmful. The "ozone layer", a region of high O_3 concentrations, is in the stratosphere where the O_3 maximum is at altitudes of ~ 30 km. The concentration and thickness of the layer is largely dependent on latitude because of differences in incoming solar radiation and atmospheric transport (Seinfeld et al., 1998). The ozone layer is formed by absorption of ultra violet (UV) light (R1.4, R1.8) and thus incoming solar UV radiation (primarily UV-B) is filtered by the ozone layer. This filtering is important because UV-B is harmful to life because the energy is capable of damaging DNA (Suzanne Clancy, 2008). In the troposphere, O_3 acts as an atmospheric cleanser through radical chemistry, ultimately removing other atmospheric species such as nitrogen oxides (NO_x), SO_2 , and volatile organic compounds (VOCs). However, excess tropospheric O_3 can be detrimental. When its concentration exceeds ~ 75 ppbv, it is considered a hazard to public health and a warning is issued (EPA, 2012a). This is because prolonged exposure to such high

concentrations can cause severe respiratory illnesses by damaging lung tissues through oxidation (EPA, 2013). Elevated O₃ concentrations also lead to particulate formation, which can also cause respiratory problems since fine particles are not effectively filtered by the body's respiratory system (Brown et al., 1950). O₃ also damages plants through oxidation and results in lower crop yields (Zhaozhong Feng et al., 2009). Additionally, O₃ absorbs infrared (IR) radiation and thus impacts global climate as an effective greenhouse gas. These factors make O₃ a very important molecule in the atmosphere, making it important to understand the details of its formation.

The concentration of O₃ in the atmosphere is often measured as the total amount present in the entire atmospheric column. This is achieved using satellite measurements or balloon instruments. Total O₃ thickness is measured in Dobson units (DU), which is equal to the thickness of a layer of pure O₃, in hundredths of a mm, if it is condensed over a unit area at 273.15K and 101.3kPa (STP). The amount of total O₃ directly relates to the amount of UV light that is filtered before reaching the surface. The Beer-Lambert law (Eq 1.1) is used to determine surface UV intensity (I) of a single wavelength relative to the incoming radiation (I₀) and depends on the O₃ depth (d), O₃'s absorption cross section at that wavelength (σ), and the O₃ number density (N).

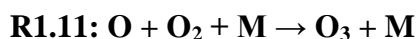
$$\text{Eq 1.1: } I = I_0 e^{-\sigma N d}$$

The Dobson unit provides the O₃ number densities at different altitudes to the number density of an ideal gas at STP and path length (d); DU = Nd. As a wide range of wavelengths are absorbed, total UV attenuation is calculated by integrating Eq 1.1 over all wavelengths. O₂ and O₃ effectively absorb the entire UV-C region while ~45W/m² and ~4W/m² reach the surface for the UV-A and UV-B region respectively (J.L.Pinedo V.

et al., 2006). In equatorial regions O_3 optical depth is measured to be ~ 260 DU which corresponds to 0.09% of UV-B and 99.3% of UV-A light reaching the surface. At the mid latitudes, (400 DU) 0.002% and 98.9% of the UV-B and UV-A region reaches the surface (Dutsch, 1973). However, the Dobson unit does not provide any details about the vertical distribution of O_3 , so balloon based measurements of O_3 mixing ratios (in parts per million by volume (ppm_v)) are used to find where O_3 is most abundant in the atmospheric column (Krankowsky et al., 2000; Mauersberger et al., 1993; Schueler et al., 1990).

1.1 Ozone in the Troposphere

O_3 in the troposphere is catalytically produced by nitrogen oxides (NO_x). Free O atoms are the limiting reactant in O_3 formation. Since UV flux ($<240\text{nm}$) is almost entirely filtered out in the stratosphere, tropospheric oxygen atoms are not formed by photolysis of O_2 (Seinfeld et al., 1998). Instead, O comes from photolysis of precursor molecules, primarily NO_2 (R1.1). NO_2 is photolyzed by wavelengths shorter than 400nm resulting in an NO molecule and a free oxygen atom. The O can react with other molecules but mainly produces O_3 via R1.11. NO_2 is primarily a product of anthropogenic emissions and areas with high NO_2 pollution also tend to have elevated O_3 levels (Sanford Sillman et al., 1990). O_3 then reacts with NO to produce NO_2 and the process continues (R1.2) and is known as the NO_x cycle (R1.1-R1.2).





O₃'s mixing ratio is also a function of VOC mixing ratios. HO₂ or organoperoxy radicals (ROO) oxidize NO into NO₂ without consuming O₃ (R1.3). Therefore, while the NO_x cycle forms and destroys O₃, the presence of HO_x and VOCs will amplify O₃ production using NO_x as a catalyst (Fig 1.2). The ratio of NO_x to VOC is important in determining O₃ equilibrium concentrations (Fig 1.2) as high tropospheric O₃ requires VOCs to be present (Sillman, 1999).

O₃ is critical in many tropospheric oxidation reactions because it produces OH radicals. OH's high reactivity drives tropospheric radical chemistry and it removes compounds like VOC's and NO_x (R1.10). An OH radical is formed when an O(¹D) reacts with water (R1.9) and O₃ photolysis is the primary source of O(¹D). O₃ photolyzes (<310nm) in the troposphere and produces an excited O(¹D) atom (Y. Matsumi et al., 2002). While O₃ can photolyze at less energetic wavelengths, at wavelengths longer than 310nm the O(¹D) quantum yield is diminished rapidly to below 0.01 (Y. Matsumi et al., 2002). Longer wavelengths (Chappuis band) will yield less energetic O(³P).



The cyclical production and destruction of O₃ with NO_x only terminates with the formation of nitric acid (HNO₃) (Fig 1.1, R1.10).

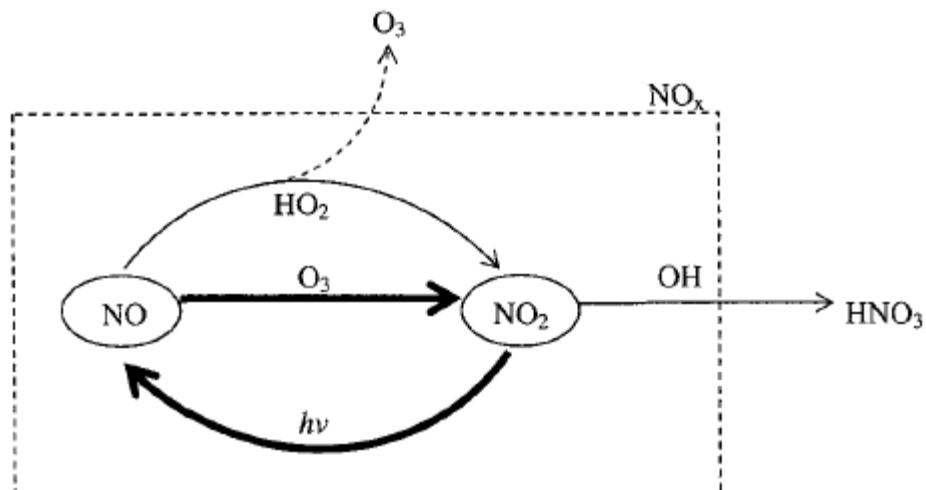


Figure 1.1: NO_x cycle and peroxy radical O₃ formation(Seinfeld and Pandis, 1998).

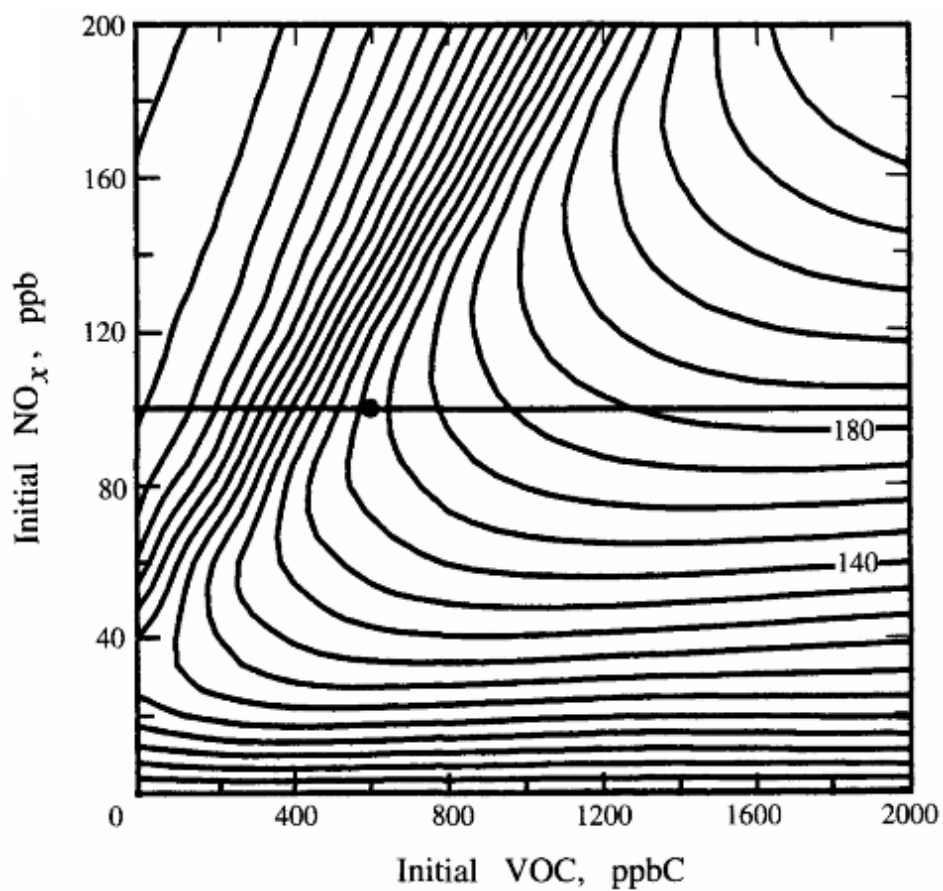
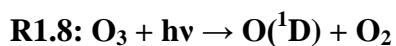
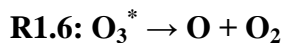


Figure 1.2: O₃ isopleths for varied NO_x/VOC ratios(Jeffries and R Crouse, 1991)

1.2 Stratospheric Ozone

In the stratosphere, O_3 is produced and destroyed in a cyclical reaction mechanism called the Chapman Cycle. O_2 is first photolyzed to two O atoms (R1.4) at wavelengths shorter than 240nm. The O atoms then react with an O_2 molecule to produce an excited state O_3^* molecule (R1.5). The excited O_3^* can then either be stabilized by collision with a third body (M) to form a stable O_3 molecule (R1.7) or dissociate back to O and O_2 (R1.6). O_3^* has a short lifetime (picoseconds) and differences in the lifetime of isotopically substituted O_3^* has been suggested as the source of O_3 's unique isotopic signature (Chapter 2)(Mauersberger K. et al., 2005). Once quenched, ground state O_3 has a substantially longer lifetime (months) which allows for it to be transported and react with many other atmospheric species.



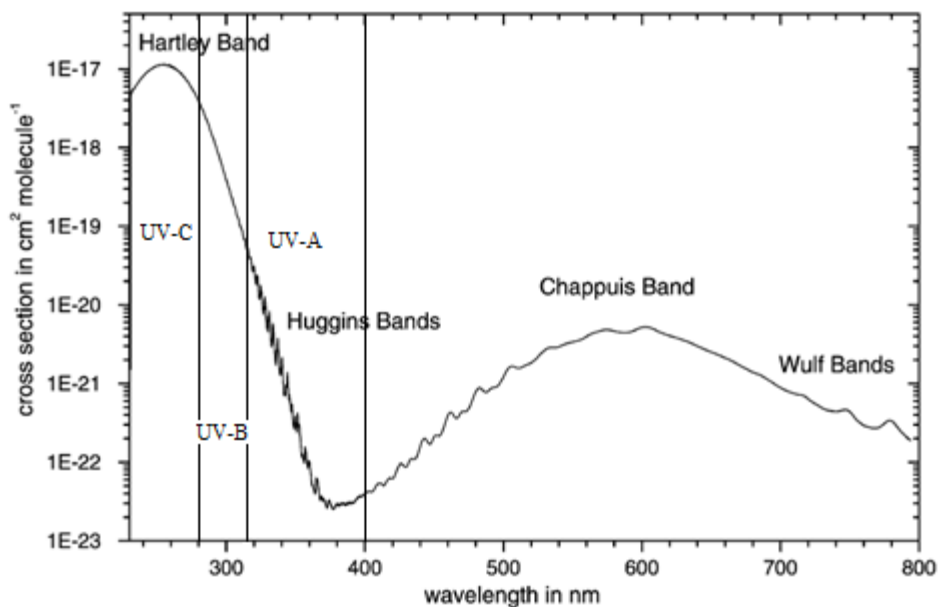


Figure 1.3: O₃ absorption spectrum (J.Orphal, 2002)

O₂ and O₃ photolysis is responsible for UV filtering in the upper atmosphere. O₂ photolyzes in the UV-C region (280-100nm) while O₃ absorbs in the Hartley band (315-280nm)(Fig 1.3) with peak absorption occurring near 256nm. O₃ photodissociation will also occur less efficiently at wavelengths up to ~330nm(J.P.Burrows et al., 1999). Shorter wavelengths (<300nm) photolyze O₃ yielding O(¹D) which drives radical chemistry through OH production. Absorption at longer wavelengths in the Chappuis and Wolf band also serve to filter some light in the visible region but do not have a significant effect on O₃ chemistry. Reactions 1.4 and 1.8 are almost entirely responsible for UV removal and if the ozone layer were to be diminished due to anthropogenic emissions, then a much greater concentration of UV light would reach the surface(F.Sherwood Rowland, 2006).

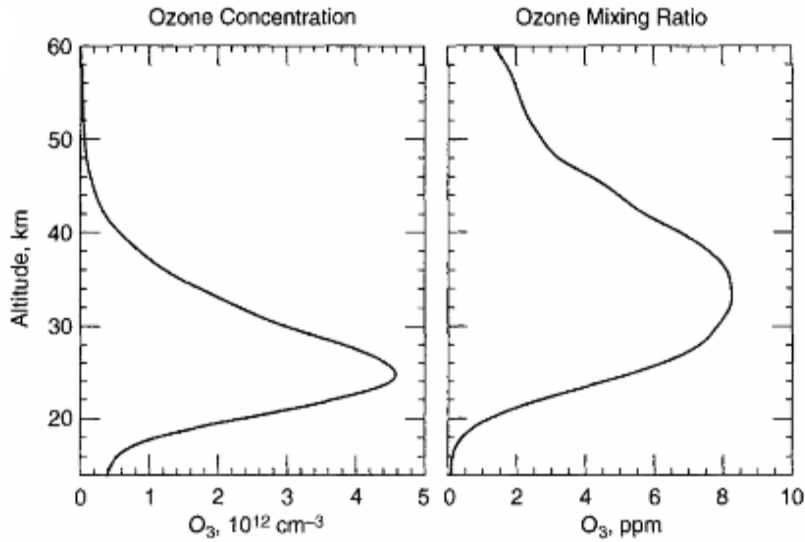
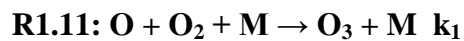


Figure 1.4: O_3 concentration with altitude (Seinfeld and Pandis, 1998).

The vertical distribution of O_3 (Fig 1.4) shows a pronounced increase at ~ 25 km and Eq 1.2 can be used to understand why this occurs. Mixing ratios in the stratosphere peak around 10 ppm_v at altitudes near 30km and total number density peaks near 25km. The rate equation for O_3 production (Eq 1.2) is a third order reaction, where k_1 is a rate constant in $\frac{cm^6}{molecules^2 * s}$ and the concentrations of the reactants O, O_2 , and M (any third body) are given in $\frac{molecules}{cm^3}$. This shows that O_3 formation rates are a function of pressure. The UV flux determines the photolysis rate constant (j_1) which produce O atoms (Eq 1.3).



$$\mathbf{Eq 1.2: \frac{d[O_3]}{dt} = k_1[O][O_2][M]}$$

$$\mathbf{Eq 1.3: 2 * \frac{d[O]}{dt} = j_1[O_2]}$$

Pressure describes the amount the amount of molecules in a given volume at a given temperature. Since pressure, and therefore $[M]$, decreases with increasing altitude, O_3

concentration is expected to decrease with $[M]$. However, $[M]$ (10^{18} molecules/cm³) is not the limiting reactant and O (10^8 molecules/cm³) production has a greater effect on increasing O₃ production rates as it will quickly react with available O₂. The rate of a 3-body reaction (R1.11) does not increase with increasing temperature like two body reactions. It is actually a net reaction of two separate reactions (R1.5 and R1.7) which are differently effected by temperature. Temperature dictates the internal energy of the excited state O₃^{*} and a greater internal energy causes O₃ production to decrease due to faster O₃^{*} decomposition. Conversely, as temperature increases, the average velocity of molecules increases, allowing for a greater number of collisions to occur and therefore allows molecules to react more frequently (Mauersberger K. et al., 2005). The temperature and pressure difference between 20km and 30km result in a 24% and 68% decrease in O₃ formation rate respectively when those conditions are calculated separately. This means while temperature has a significant effect, pressure is the dominant rate determining condition. As a result, O₃ is predominantly formed in the stratosphere where O and UV light are prevalent (Fig 1.5), yielding higher mixing ratios (~10ppmv) than in the troposphere (~10ppbv). From the number densities of O(³P) observed (Fig 1.5), the rate of O₃ formation (Eq 1.2, $k_1=6 \times 10^{-34}$) is calculated to be 3.04×10^{10} molecules/cm³s at 30km and 3.21×10^{10} molecules/cm³s at 32km (S.P.Sander et al., 2003).

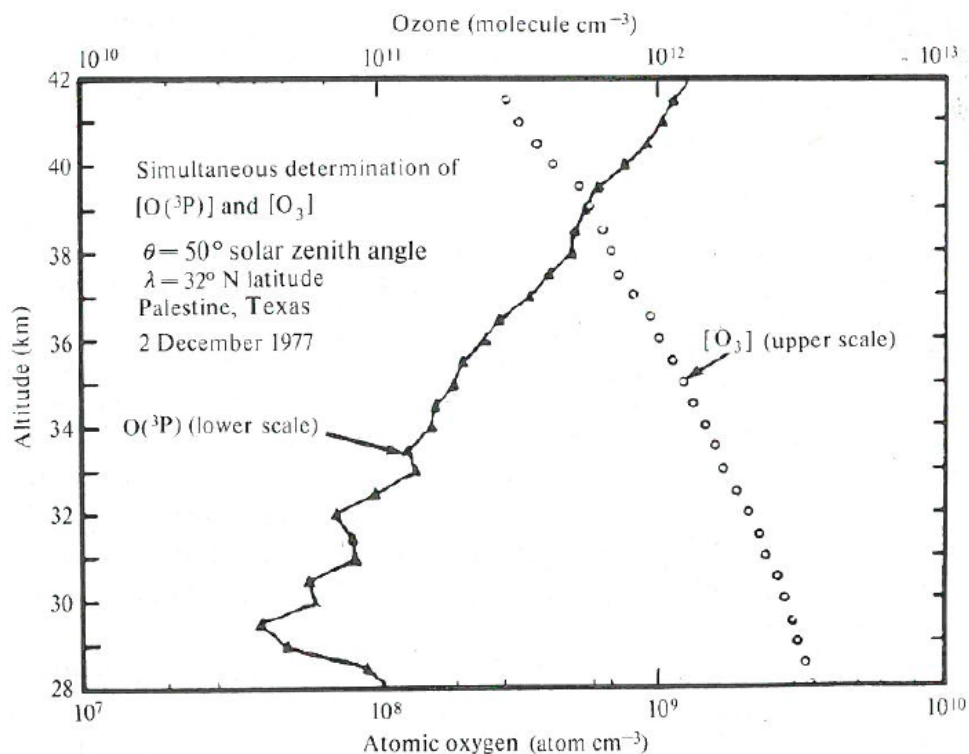


Figure 1.5: O and O_3 number densities in the stratosphere (Wayne, 1996).

1.3 Oxygen Isotopic Variations

O_3 has intriguing isotopic compositions and distributions. Atoms that contain different number of neutrons but the same number of protons are called isotopes of the same element. For example, oxygen atoms are defined as a nucleus that contained 8 protons which each contribute a mass of 1amu. The remaining mass is primarily the number neutrons (1amu each) and a minute fraction of mass comes from the electrons ($\sim 5 \times 10^{-4}$ amu). Isotopes can have unstable or stable nuclei. Unstable isotopes decompose or radioactively decay and the time at which half of the initial nuclei have decayed is called its half-life. Stable isotopes do not decay and thus are useful tracers because they have an infinite lifetime and are integrated into many different molecules. Their different masses allow the isotopic concentration in various molecules to be quantitatively

assessed by mass spectrometry(Edmond de Hoffman et al., 2007). Differences in isotope abundances can be used to understand the reaction mechanisms by which a molecule, such as O₃, is formed.

Isotope abundances are typically measured as ratios and expressed in delta notation (δ). Minor isotopes, ¹⁷O and ¹⁸O for oxygen, are compared to the major isotope (¹⁶O) and are reported as a ratio (Eq 1.4). Changes in oxygen isotopic abundance are calculated by comparison of isotope ratios of a sample and standard of known isotopic composition and multiplied by 1000 to present the value in permil (‰) (Eq 1.5)(Criss, 1999).

$$\text{Eq 1.4: } R^{17} = \frac{{}^{17}\text{O}}{{}^{16}\text{O}}$$

$$\text{Eq 1.5: } \delta^x\text{O}(\text{‰}) = \left(\frac{R_{\text{sample}}}{R_{\text{standard}}} - 1 \right) * 1000$$

The reference standard used for oxygen isotope abundances is Vienna Standard Mean Ocean Water (VSMOW) that has a known isotopic composition that is ¹⁷O/¹⁶O = 3.790x10⁻⁴, ¹⁸O/¹⁶O = 2.0004x10⁻³(NIST, 2005). When compared to VSMOW, most oxygen containing molecules, like O₂ ($\delta^{17}\text{O} \approx 11\text{‰}$, $\delta^{18}\text{O} \approx 23\text{‰}$), water vapor ($\delta^{17}\text{O} \approx -1$ to -15‰ , $\delta^{18}\text{O} \approx -2$ to -30‰), and silicates ($\delta^{17}\text{O} \approx -5$ to 13‰ , $\delta^{18}\text{O} \approx -10$ to 26‰) have $\delta^{17}\text{O}$ and $\delta^{18}\text{O}$ below 50‰ (Gabriel Bowen, 2013;Ryoji Tanaka et al., 2013). In contrast, O₃'s isotopic composition often exceeds 100‰(Mauersberger et al., 2001).

Isotopic enrichments or depletions are caused by the difference in physical properties related to the unequal mass of the isotopically substituted molecules(Criss, 1999). This is called isotopic fractionation and the magnitude of fractionation is described by a fractionation factor, α (Eq 1.6). α is calculated as a ratio of any two R

values (Eq 1.6) arising during a single process. This can be the ratio of reactant and product R values in a chemical reaction or a phase change (e.g. water→gas). Isotope enrichments or depletions are also quantified by ϵ can also be expressed in permil and are related to α by Eq 1.7(Criss, 1999). α and ϵ are used to describe both a change from starting material to final product as well as change in equilibrium processes.

Fractionation that occurs in an equilibrium process often results from a phase change (R1.12-1.14), where α and α^{-1} describe the forward and reverse reaction, respectively.

Isotope fractionation in reactions where the forward reaction is unidirectional are called kinetic isotope effects (KIE).

$$\text{Eq 1.6: } \alpha = \frac{R_A}{R_B}$$

$$\text{Eq 1.7: } \epsilon = (\alpha - 1) * 1000$$

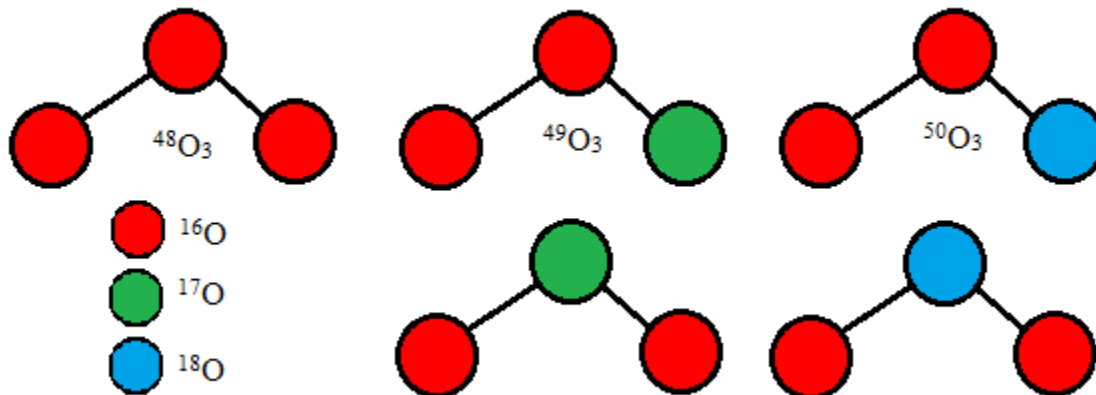


Figure 1.6: Ozone's isotopic forms

α also describes the ratio of production/destruction rates of isotopologues and isotopomers. An isotopologue (isotope homologue) is any molecule that is elementally identical but at least one of the atoms is isotopically different, meaning isotopologues

have different masses. An isotopomer (isotope isomer) is any molecule that is elementally and isotopically identical but the position of at least one atom is different, meaning isotopomers have the same mass. Figure 1.6 shows all major forms of O_3 of which there are 3 isotopologues ($^{48}O_3$, $^{49}O_3$, $^{50}O_3$) and two isotopomers (asymmetric and symmetric) for both $^{49}O_3$ and $^{50}O_3$. While double and triple substituted isotopologues of O_3 exist, their concentrations are so minute that they are essentially irrelevant in most natural systems.

Isotopologues and isotopomers react with other molecules at different rates and also form/decompose at different rates which are examples of kinetic isotope effects (KIE) (Mauersberger et al., 1999). O_3^* (R1.5) formation is described by the rate law (Eq 1.8) and has a rate constant (k_{48}); similar rate laws can be written for the other O_3 isotopologues and isotopomers (Eq 1.9-1.12). The magnitude of the isotopic fractionation is directly related to the differences in the rate constants. This ratio is usually $\alpha \approx 1$ but the deviation from 1 in the thousandths is measurable and can describe the reaction, exchange, or decomposition that a molecule has undergone (Michalski et al., 2004).

$$\text{Eq 1.8: } \frac{d[O_3^*]}{dt} = k_{48} [^{16}O] [^{32}O_2]$$

$$\text{Eq 1.9: } \frac{d[O_3^*]}{dt} = k_{49} [^{16}O] [^{33}O_2]$$

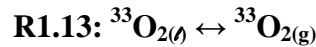
$$\text{Eq 1.10: } \frac{d[O_3^*]}{dt} = k_{49} [^{17}O] [^{32}O_2]$$

$$\text{Eq 1.11: } \frac{d[O_3^*]}{dt} = k_{50} [^{16}O] [^{34}O_2]$$

$$\text{Eq 1.12: } \frac{d[O_3^*]}{dt} = k_{50} [^{18}O] [^{32}O_2]$$

$$\text{Eq 1.13: } \alpha = \frac{k_{50O_3}}{k_{48O_3}}$$

Equilibrium isotopic fractionation occurs during phase changes or chemical equilibrium and the magnitude of fractionation is directly related to the difference in mass of the isotopologues (Criss, 1999). For example, when equilibrium between O₂ gas and liquid is reached, the liquid O₂ reservoir becomes enriched while the O₂ gas is depleted. This is because the isotopically lighter ¹⁶O¹⁶O molecule will preferentially ($K_{32} > K_{33} > K_{34}$) evaporate compared to the ¹⁶O¹⁷O and ¹⁶O¹⁸O molecules (R1.12-R1.14). The phase change equilibrium means that k_{32} (Eq 1.14) describes the rate from liquid to gas and the inverse reaction will just be k_{eq32}^{-1} . Typically, as the mass difference between two isotopes gets larger the observed fractionation becomes larger. So, while the mass difference is relatively small in oxygen (1/16th of total mass), lighter species like hydrogen experience a mass difference (between ¹H and ²H) that is much greater and results in substantially larger enrichments (Criss, 1999).



$$\mathbf{Eq 1.14: } \frac{d[^{32}\text{O}_{2(g)}]}{dt} = k_{eq32} [^{32}\text{O}_{2(l)}]$$

$$\mathbf{Eq 1.15: } \alpha_{l \rightarrow g} = \frac{k_{eq34}}{k_{eq32}}$$

$$\mathbf{Eq 1.16: } \frac{\delta^{17}\text{O}}{\delta^{18}\text{O}} = \frac{\alpha_{17}}{\alpha_{18}} = \frac{(k_{17}/k_{16})}{(k_{18}/k_{16})} \approx 0.52$$

In elements with two heavy isotopes such as oxygen, the substituted species tends to enrich very predictably based on the mass difference between ¹⁷O and ¹⁸O. Most oxygen containing molecules have a ratio of $\delta^{17}\text{O}/\delta^{18}\text{O} \approx 0.52$ (M.F. Miller et al., 1999).

This is known as mass dependent fractionation and a similar ratio (λ) is observed in almost all natural samples. The value arises as isotope fractionations are mainly a function of vibrational energy. Molecular vibrations can be approximated using the simple harmonic oscillator (SHO) where two atoms can be considered to be attached by a spring (bond) and their vibrational energies are related to the reduced mass of the diatomic molecule (Eq 1.17). Fractionation is largely determined by the difference in the molecule's zero point energy (lowest vibrational energy level) which is also determined by the reduced mass of the molecule. For diatomic oxygen (^{16}O , ^{17}O , ^{18}O), the reduced mass difference will change depending on what atom the O is bound to. So for O_2 , $\lambda=0.515$, but if oxygen is bound to ^1H , ^{56}Fe , and ^{238}U , $\lambda=0.5267$, 0.5048 , and 0.5021 , respectively (Eq 1.18). There are a variety of published values for the mass dependent ratio (0.51-0.53)(M.F.Miller et al., 1999; Matsuhisa et al., 1978), known as the terrestrial fractionation line (TFL), which has been shown to be process dependent. As a result, creation of a single value to apply to all natural samples is unlikely to be agreed upon (Miller, 2002).

$$\text{Eq 1.17: } \mu = \frac{m_1 m_2}{m_1 + m_2}$$

$$\text{Eq 1.18: } \lambda = \frac{(\mu_2/\mu_1)^{-1}}{(\mu_3/\mu_1)^{-1}}$$

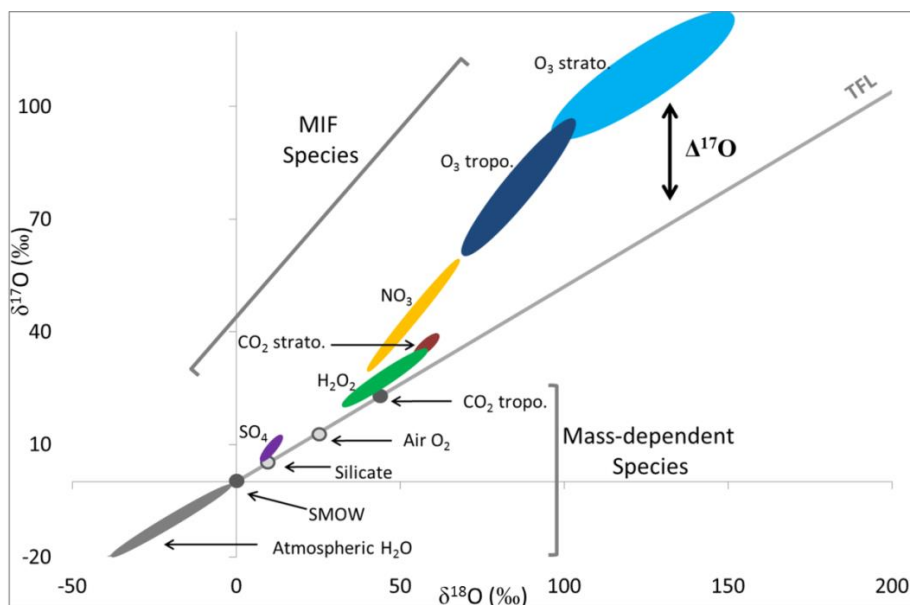


Figure 1.7: Terrestrial Fractionation Line(TFL) and other characterized atmospheric species(Krystin Riha, 2013)

1.4 Mass Independent Fractionation and Enrichment of Ozone

Not all oxygen isotopic measurements fall on the TFL, in particular O_3 and products from reaction with O_3 (NO_3^- , SO_4^{2-}) do not follow the 0.52 ratio (fig 1.7). O_3 formation fractionates mass independently, i.e. the $\delta^{17}O/\delta^{18}O$ slope is 1. $\Delta^{17}O$ is the calculated difference in isotopic enrichment between the observed $\delta^{17}O/\delta^{18}O$ ratio and the TFL(Thiemens, 2006). While O_3 creates its own $\Delta^{17}O$ signature, the molecules it reacts with simply have that signal transferred to them. For example, when nitrite ($\Delta^{17}O=0$) reacts with O_3 (Chapter 2), it forms nitrate that has a $\Delta^{17}O$ value $1/3 \Delta^{17}O$ of the abstracted oxygen atom since only 1 in 3 O atoms came from reaction with O_3 (William C.Vicars et al., 2012).

$$\text{Eq 1.19: } \Delta^{17}O = \delta^{17}O - (\lambda * \delta^{18}O)$$

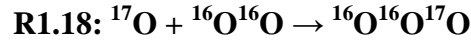
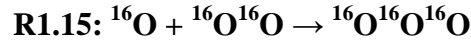
$$\text{Eq 1.20: } \Delta^{17}O = 1000 \ln \left(1 + \frac{\delta^{17}O}{1000} \right) - \lambda 1000 \ln \left(1 + \frac{\delta^{18}O}{1000} \right)$$

Equation 1.19 is the linear approximation of $\Delta^{17}\text{O}$ with λ (0.52) equal to the expected mass dependent fractionation ratio. Isotopic enrichment is a natural logarithmic function so over a narrow range of enrichment, the approximation will provide a reasonably accurate value, but when making comparisons between studies and over a large range of enrichments the robustness of the equation is insufficient (Miller, 2002). λ is process dependent and therefore cannot be considered to be a single value rather it can range from 0.51 – 0.53. This will be discussed in greater detail in Chapter 2 along with a description of why Eq 1.20 should be used for calculating $\Delta^{17}\text{O}$. Most systems will not have a single mass dependent reaction but when the rate of reactions are considered, there may be a kinetically dominant reaction in which case the λ of that reaction alone can be used as λ for the approximation of $\Delta^{17}\text{O}$ (Kaye et al., 1983; Morton et al., 1990).

O_3 was the first terrestrial compound to have a measured non-zero $\Delta^{17}\text{O}$ and is considered to be the primary source of all $\Delta^{17}\text{O}$ signatures in other atmospheric compounds (Heidenreich, III et al., 1983). O_3 will sometimes reach an isotopic equilibrium with some atmospheric molecules. Therefore, the amount of $\Delta^{17}\text{O}$ signal transferred to the product molecule will be dependent on the rate at which that isotopic equilibrium is reached. The magnitude of $\delta^{17}\text{O}$, $\delta^{18}\text{O}$, and $\Delta^{17}\text{O}$ enrichment in O_3 depends on its formation temperature and pressure as those conditions determine the rate of quenching of O_3^* (Janssen et al., 2002; Morton et al., 1990). The energetically excited O_3^* molecule must be quenched to become stable and it has been suggested that this step is the origin of the mass independent signature (Heidenreich et al., 1986).

Current theory postulates that the symmetry of O_3^* influences its lifetime. When O_3 is formed with all ^{16}O atoms resulting in $^{48}\text{O}_3$, the molecule is symmetric (R1.15).

However, when ^{17}O or ^{18}O is added, symmetric (R1.16, R1.19) and asymmetric (R1.17, R1.18, R1.20, R1.21) forms of $^{49}\text{O}_3$ or $^{50}\text{O}_3$ are produced (Fig 1.6).



The asymmetric form of O_3 has a greater density of energy states which allows for the excited state molecule to exist longer before decomposition (R1.7) (Gao et al., 2001). This longer lifetime in asymmetric O_3^* is achieved regardless of whether it is ^{17}O or ^{18}O in the terminal position of the O_3 molecule and will exhibit mass independent enrichment (Gao et al., 2002; Heidenrich et al., 1986). As long as the mass of both terminal atoms is not equal, the mass of the terminal atom is inconsequential.

It is assumed that if each pathway of the Chapman cycle could be separated that all would have $\frac{\alpha_{17}}{\alpha_{18}} = 0.52$ with the exception of R1.7 which fractionates mass independently (Gao et al., 2001). If this reaction could be isolated, one would expect that the longer lifetime of the asymmetric species, and therefore the higher rate of quenching, to form stable O_3 would result in $\frac{\alpha_{17}}{\alpha_{18}} \approx 1$. Equations 1.21, 1.22, and 1.23 demonstrate the isotope specific rate equations and for R1.15, 1.17 and 1.20 respectively.

$$\mathbf{Eq\ 1.21: } \frac{d[^{48}\text{O}_3]}{dt} = k_{16} [^{32}\text{O}_2] [^{16}\text{O}]$$

$$\text{Eq 1.22: } \frac{d[^{49}\text{O}_3]}{dt} = k_{17}[^{33}\text{O}_2][^{16}\text{O}]$$

$$\text{Eq 1.23: } \frac{d[^{50}\text{O}_3]}{dt} = k_{18}[^{34}\text{O}_2][^{16}\text{O}]$$

$$\text{Eq 1.24: } \frac{\delta^{17}\text{O}^a}{\delta^{18}\text{O}^a} = \frac{\alpha_{17}}{\alpha_{18}} = \frac{(k_{17}/k_{16})}{(k_{18}/k_{16})} \approx 1$$

The isotope specific rate equations are the same as any other rate equation that does not take mass of each element into account but where they differ is that the same reaction is broken down into individual pathways despite each reaction resulting in O₃. Equation 1.24 demonstrates that when looking at the enrichment of only asymmetric O₃ (δ¹⁷O^a and δ¹⁸O^a), the ratio of rate constants to compare alphas can be used, but in this case, enrichment is shown to be mass independent.

1.5 Application of Predicted and Measured Ozone Isotopic Enrichment

Application of laboratory relationships between temperature, pressure and isotopic enrichment in O₃ formation could be used to help better understand reaction rates and mechanisms (Janssen et al., 2002; Mauersberger et al., 1999). O₃'s isotopic composition in the stratosphere was first directly measured in the early 1980's but the data was later shown to be unreliable (δ¹⁸O=400‰)(Mauersberger, 1981). Later balloon measurements, which used improved sampling methods and instrumentation, resulted in values much closer to the laboratory predicted values (Krankowsky et al., 2000; Mauersberger, 1981; Mauersberger et al., 1993). While the error was still relatively high, the data in Appendix Table 1 shows that at very high altitudes, isotopic enrichment of both ¹⁷O and ¹⁸O often exceeds of 100%. A more detailed laboratory examination is

then absolutely necessary as isotopic enrichments of that magnitude are almost never seen in any other oxygen containing natural sample.

Measured O₃ isotopes in the troposphere also showed an exceedingly large enrichment ($\delta^{17}\text{O}=56.5\text{-}86.6\text{‰}$, $\delta^{18}\text{O}=69.9\text{-}96.1\text{‰}$, Appendix Table 2) which then raises the question: How do temperature and pressure conditions truly affect total O₃ enrichment?(Johnston et al., 1997;William C.Vicars et al., 2012) The conditions of the stratosphere and troposphere are drastically different as the stratosphere typically has temperatures below 240K and pressures nearly 2 orders of magnitude below surface pressure (~10 torr)(C.David et al., 2012). Because enrichment decreases with decreasing temperature and increasing pressure, the expected effect with increasing altitude would at least be partially offset(Morton et al., 1990). However, O₃ signal is not constant in any one location or time as pressure and temperature are constantly changing which will change O₃'s isotopic enrichment.

This thesis will focus on the temperature and pressure dependent enrichment of O₃ which could lead to better understanding of isotopic variation in atmospheric molecules. Both $\delta^{17}\text{O}$ and $\delta^{18}\text{O}$ in O₃ vary with temperature and pressure of formation and while most oxygen isotope studies focus on $\delta^{18}\text{O}$ and simply infer $\delta^{17}\text{O}$ from an expected mass dependent relationship which can be misleading as variation of $\delta^{17}\text{O}/\delta^{18}\text{O}$ ratios can provide valuable insight into what reactions or exchange processes a molecule has undergone. Specifically, in the troposphere, O₃ will undergo many more oxidation reactions with varied atmospheric species (NO_x, HO_x, SO_x) and transfer its mass independent isotopic signature to those species through oxygen abstraction(Thiemens, 2006). This serves as a useful tracer to better understand atmospheric chemistry because

if $\Delta^{17}\text{O}$ of O_3 is known, then the signal will only be fractionally diluted with future reactions.

Since O_3 will almost exclusively undergo reactions by its terminal atom, the isotopic enrichment of the terminal atom must be understood independently (William C. Vicars et al., 2012). Also, as symmetry of the O_3^* molecule is postulated to be the source of the mass independent signal, an examination combining the previous work on temperature and pressure dependent O_3 formation and the effects of symmetry should provide an explanation for temperature and pressure dependent terminal enrichment (C. Janssen, 2005; Heidenrich et al., 1986; Janssen et al., 2002). All of these factors must be examined in order to gain a better understanding of atmospheric chemistry and when considering examples of $\Delta^{17}\text{O} > 0$, one must first be able to predict how temperature and pressure changes O_3 's bulk and terminal isotopic enrichment.

.

CHAPTER 2. TEMPERATURE DEPENDENT ENRICHMENT OF OZONE

2.1 Introduction

Ozone's isotopic enrichment has been examined over a wide range of temperatures and pressures but conditions of the troposphere are particularly important as O_3 is a major oxidant in many lower atmosphere reactions. Higher concentrations of stratospheric O_3 and the importance of the ozone layer were the basis for studying O_3 's extreme isotopic enrichment (Krankowsky et al., 2000; Mauersberger et al., 1993; Schueler et al., 1990). However, temperature dependent isotopic enrichment experiments had poor precision and were limited to pressure conditions typical of the stratosphere. However, O_3 is also important in the troposphere as an oxidizer in many reactions. As a result, O_3 's unique isotopic signature is transferred to a variety of atmospheric molecules, such as NO_3^- and SO_4^{2-} , and can be used as a tracer for NO_x and SO_2 oxidation mechanisms (Costa et al., 2011; Kunasek et al., 2010; Savarino et al., 2013; Sofen et al., 2011). Since the transferred isotopic signature will mirror that of O_3 , the effect of tropospheric temperature and pressure conditions on O_3 isotopic enrichment needs to be examined in the laboratory.

Previous laboratory studies of the isotopic composition of O_3 produced O_3 at low pressures, in closed systems, or with starting gas heavily enriched in ^{17}O and ^{18}O

(Janssen et al., 2001; Mauersberger et al., 1999; Morton et al., 1990; Thiemens et al., 1988; Wolf et al., 2000). These conditions do not replicate the lower atmosphere where pressure is 760 torr, the system is open, and the starting gas reservoir has minor enrichment ($\delta^{17}\text{O} \approx 12\text{‰}$, $\delta^{18}\text{O} \approx 23\text{‰}$) and considered infinite (Criss, 1999). An O_3 production apparatus (Section 2.2) that uses photolysis as the driving force for the Chapman Cycle and a non-static and approximately infinite reservoir should limit the potential isotope effects from oxygen recycling and vessel wall interactions.

O_3 's formation in the troposphere is not as simplistic as the Chapman reactions (Section 1.3) examined in this study. Many more O_3 chemical destruction reactions occur in the troposphere. However, they should only affect O_3 's steady state concentration and have a small impact on its isotopic signature because O_3 's isotopic enrichment is assumed to mainly occur during the recombination reaction (Janssen et al., 2002; Mauersberger et al., 1999). Also, O atoms in the troposphere are primarily derived from NO_x photolysis. This will alter the starting isotopic composition of oxygen atoms used in O_3 formation but relative to the isotopic composition of the starting gas, the net change in isotopic enrichment should remain the same because of $\text{O} + \text{O}_2$ exchange reactions. This chapter details an experiment that assesses the isotopic enrichment of O_3 as a function of temperature and conducted at a tropospheric relevant pressure in a flow system.

2.2 Experimental Setup

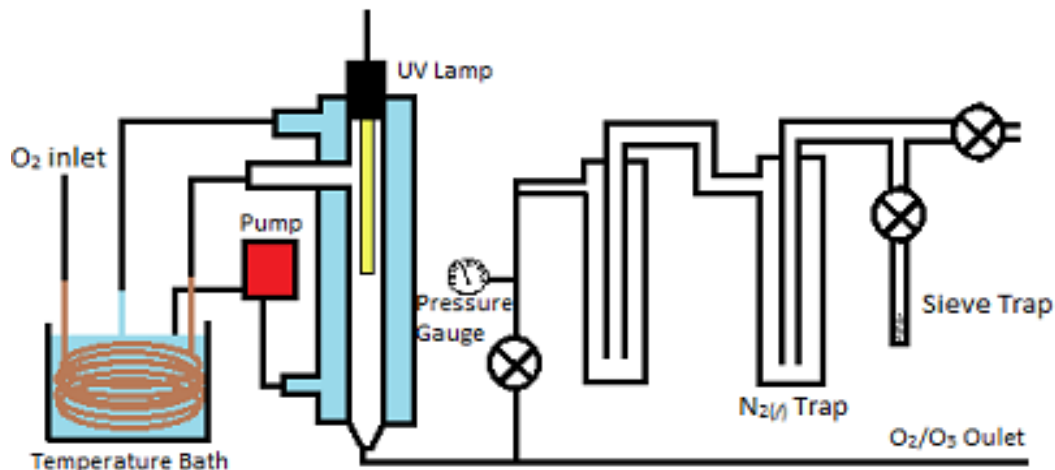


Figure 2.1: O₃ formation and collection apparatus

O₃ was generated and collected using the apparatus shown in Figure 2.1. The goal was to produce O₃ over a range of tropospheric temperatures (273K-320K) at pressures near 760 torr and then determine its isotopic composition. A steady state concentration of O₃ was produced from a flow of temperature controlled O₂ gas. The O₂ source was a tank of compressed research grade oxygen (99.99+% pure) from Airgas. The O₂ flowed from the tank through the inlet (Fig 2.1) using positive pressure (765 torr) at a rate of ~1.5 L/min that was regulated using an Omega flow meter. The O₂ gas first passed through a long copper coil submerged in a constant temperature bath, before passing through a UV photolysis chamber (Fig 2.1) that was also temperature controlled by pumping the bath water through its water jacket. The temperature conditioning is necessary to ensure that the O₂ was not significantly heated during the photolysis reactions. The temperature controlled bath water was monitored and adjusted when necessary (± 1 K).

The light source was a Pen Ray Hg vapor lamp. The emission spectrum of the UV source (Fig 2.2) shows that the primary output is at 254nm with minimal output at longer wavelengths and a small emission line at 185 nm. 254nm is known to be very near O₃ peak absorption, while 185 nm light dissociates O₂. This spectral asymmetry leads to a high rate of O₃ photolysis relative to O₂ photolysis. Exposure to the UV light source was ~2s based on the flow rate of 1.5 L/min and a chamber volume of 50 mL. The gas exiting the chamber was monitored for O₃ concentrations using a 2B Technologies O₃ monitor. Tests showed that the UV light source required a 2 minute warm up period to reach peak output and produced consistent O₃ concentrations. After this warm up period a steady O₃ concentration of 48 +/- 0.3ppm_v was produced.

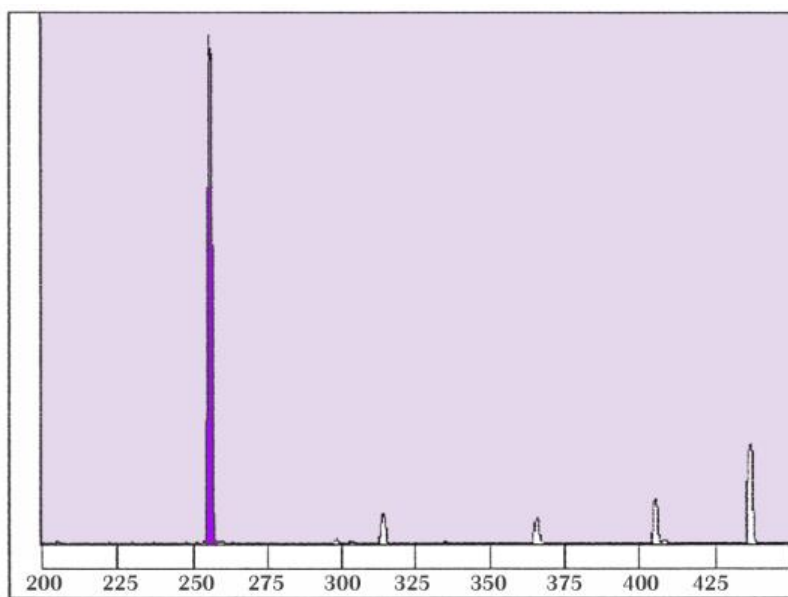


Figure 2.2: Pen-Ray mercury lamp emission spectra (UVP, 2014).

Cryogenic collection of O₃ required a series of condensing and excess O₂ removal steps. The O₃ collection line was evacuated and the collection trap was submerged in liquid nitrogen. The needle valve (Fig 2.1) was slowly opened until pressure within the

collection line reached 100 torr. This pressure allowed for rapid sample collection without condensing unwanted O₂. For experiments conducted at temperatures between 310K and 320K, a 230K ethanol bath was placed on the first trap. High temperature trials without the ethanol bath had smaller sample sizes suggesting O₃ was bypassing the trap. O₃ was collected for 30 minutes per trial.

It is unlikely that the O₃ trapping step induced substantial alteration of the $\delta^{18}\text{O}$ or $\Delta^{17}\text{O}$ values. Assuming equilibrium between the gas and liquid O₃ phases, the ~ 100 torr total pressure and 48 ppm_v O₃ mixing ratio results in an O₃ partial pressure of 4.8 mtorr in the collection trap. AT 77K the equilibrium partial pressure of O₃ is 1.56 mtorr and indicates that 67.5% of O₃ is in the liquid phase at all times(Hanson et al., 1986). Isotope mass balance considerations and small isotope equilibrium fractionation factor for a heavy O₃ molecule suggests that the alteration of O₃ $\delta^{18}\text{O}$ values by cryogenic trapping should be minimal (Mauersberger et al., 1987). In addition, since gas-liquid equilibrium should follow mass dependent isotope rules, the $\Delta^{17}\text{O}$ values are even less likely to have been altered by the collection process. After the O₃ collection was complete the needle valve was closed and the O₃ was transferred to a sample tube. The collection line and a collection tube, containing molesieve 5A, were evacuated to below 10 mtorr. The sample tube was submerged in liquid nitrogen and the O₃ collection trap was thawed, transferring the O₃ to the collection tube, evident by a visible purple ring characteristic of condensed O₃. The transfer was considered complete when pressure reached <10mtorr. The tube was then isolated, warmed to room temperature, and the O₃ decomposed to O₂ on the molecular sieve surface. The resulting O₂ was measured for the $\delta^{17}\text{O}$ and $\delta^{18}\text{O}$ using a

Delta V Isotope Ratio Mass Spectrometer (IRMS) and a reference O₂ gas calibrated to VSMOW.

2.3 Results

The average $\delta^{17}\text{O}$, $\delta^{18}\text{O}$ and $\Delta^{17}\text{O}$ values of O₃ for each temperature trial are given in Table 2.1. All δ values are reported compared to the initial O₂ gas. The ¹⁸O and ¹⁷O isotopes were nearly equally enriched with $\delta^{18}\text{O}$ values ranging from 72.4 to 87‰ and the $\delta^{17}\text{O}$ values from 70.9 to 81.6‰. This resulted in calculated $\Delta^{17}\text{O}$ values (discussed in section 2.5.3) were between 31.7 and 34.6‰. The precision (1 σ) for $\delta^{17}\text{O}$ and $\delta^{18}\text{O}$ both averaged $\pm 1.9\text{‰}$ and never exceeded 3.1‰ for any given temperature experiment. The precision of the calculated $\Delta^{17}\text{O}$ values for all temperature points averaged $\pm 0.9\text{‰}$ and never exceeded 1.2‰. The temperature series showed that there was a linear dependence between temperature and O₃ isotopic enrichment (Eq 2.1-2.3) with the least squares regression $R^2 = 0.98, 0.99,$ and 0.96 for $\delta^{17}\text{O}, \delta^{18}\text{O}$ and $\Delta^{17}\text{O}$, respectively. Within the 47K experimental temperature range, precision of the linear approximations was $\pm 0.48\text{‰}$ for $\delta^{17}\text{O}$ and $\pm 0.56\text{‰}$ for $\delta^{18}\text{O}$.

T(K)(n)	δ^{17}	$\sigma(\delta^{17})$	δ^{18}	$\sigma(\delta^{18})$	$\Delta^{17}\text{O}$	$\sigma(\Delta^{17}\text{O})$
273(4)	70.9	2.9	72.4	3.1	31.7	1.2
283(4)	72.6	2.1	74.6	2.2	32.3	0.9
294(4)	76.8	2.4	80.0	2.3	33.5	1.1
301(5)	77.3	1.6	80.8	1.6	33.6	0.9
310(5)	80.2	1.3	84.6	1.4	34.4	0.6
320(4)	81.6	1.3	87.0	0.9	34.6	0.8

Table 2.1: O₃ enrichments relative to starting gas composition

Eq 2.1: $\delta^{17}\text{O} = 0.2385T + 5.77$

Eq 2.2: $\delta^{18}\text{O} = 0.3216T - 15.58$

Eq 2.3: $\Delta^{17}\text{O} = 0.0649T + 14.07$

2.4 Discussion

2.4.1 O + O₂ Exchange

The isotopic composition of O₃ is intimately controlled by the O + O₂ exchange reaction. The O₃ isotopologue fractionation factors for the recombination reactions cannot be obtained from measured $\delta^x\text{O}$ values relative to the composition of the starting material. Instead, these measured values represent enrichment associated with all Chapman cycle reactions, including $\text{Q} + \text{O}_2 \leftrightarrow \text{O} + \text{QO}$ exchange, where Q is the ¹⁸O isotope (similar exchange occurs for ¹⁷O = P). This exchange is the alternative pathway occurring after formation of O₃* (R2.4), with exchange occurring if O₃* decomposes back into O₂ + O rather than being stabilized to O₃. The O + O₂ (R2.1, R2.2, R2.13, R2.14) kinetic exchange rate is fast; 200 times that of the O₃ recombination rate (R2.4) (Kaye et al., 1983). This reaction causes large isotopic depletion of free O atoms affecting the overall $\delta^{17}\text{O}$ and $\delta^{18}\text{O}$ of O₃ (Kaye et al., 1983; Kaye, 1986; Morton et al., 1990).

The isotopic depletion of the O atom was calculated using the partition coefficient calculation (Eq 2.4, R2.1) (Kaye et al., 1983). Here α_{ex}^{50} (α_{ex}^{49}) is defined as the equilibrium fractionation factor for O₃ (50, 49 amu) if only O+O₂ exchange is considered, i.e. the isotope effects from photolysis or the recombination reactions are ignored. O₃ is

predicted to be isotopically depleted with the magnitude of the isotopic depletion calculated using Eq 2.6 and 2.7.

$$\text{Eq 2.4: } K_{\text{eq}} = 1.94e^{(32/T)}$$

$$\text{Eq 2.5: } K_{\text{eq}} = 1.96e^{(16.8/T)}$$



$$\text{Eq 2.6: } \alpha^{50}\text{O}_3 = \frac{2 \left(1 + \left(1.94e^{\left(\frac{32}{T(K)} \right)} \right) \right)}{3 * 1.94e^{\left(\frac{32}{T(K)} \right)}}$$

$$\text{Eq 2.7: } \alpha^{49}\text{O}_3 = \frac{2 \left(1 + \left(1.96e^{\left(\frac{16.8}{T(K)} \right)} \right) \right)}{3 * 1.96e^{\left(\frac{16.8}{T(K)} \right)}}$$

Morton performed the same O+O₂ exchange calculation as Kaye and Strobel except using ¹⁷O, which yielded Eq 2.5(R2.2)(Morton et al., 1990). Our partition coefficient calculations used updated rotational frequencies but differed by no more than 1.8‰ when compared to those of Kaye (1983), Morton (1990), and Janssen (2005) (Criss, 1999; NIST, 2012).

The O₃ recombination isotopic enrichment was calculated by subtracting the O atom depletion, calculated from the exchange reaction, from the measured O₃ enrichment (Fig 2.3). These results were compared to Morton's (1990) enrichment (Fig 2.4). In order to compare with the results of Morton et al., accounting for the difference in experimental pressures was necessary. This was done by using a polynomial fit of Morton's constant T and variable P experimental data to get at a quadratic equation that predicts the change in δ values as a function of pressure (Eq 2.8, 2.9).

Eq 2.8: $\delta^{17}\text{O} = -8.5569(\log_{10}P)^2 + 16.803(\log_{10}P) + 105.09$

Eq 2.9: $\delta^{18}\text{O} = -11.173(\log_{10}P)^2 + 22.456(\log_{10}P) + 116.13$

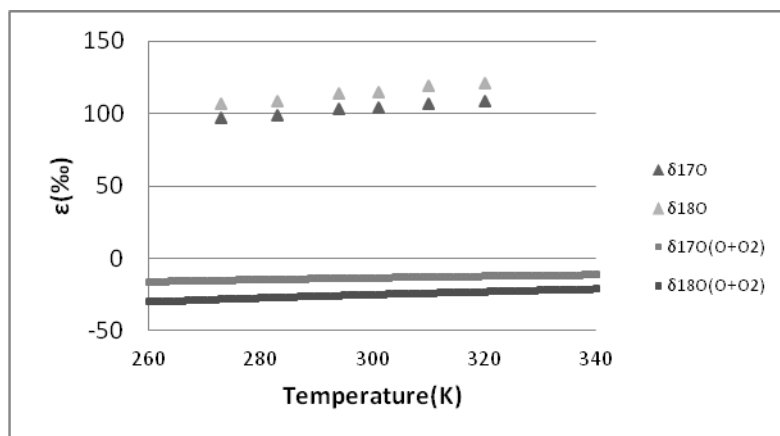


Figure 2.3 Pressure corrected O_3 enrichment (triangles) measured relative to the starting gas represents all reactions in the Chapman mechanism including a depletion associated with $\text{O}+\text{O}_2$ exchange (squares).

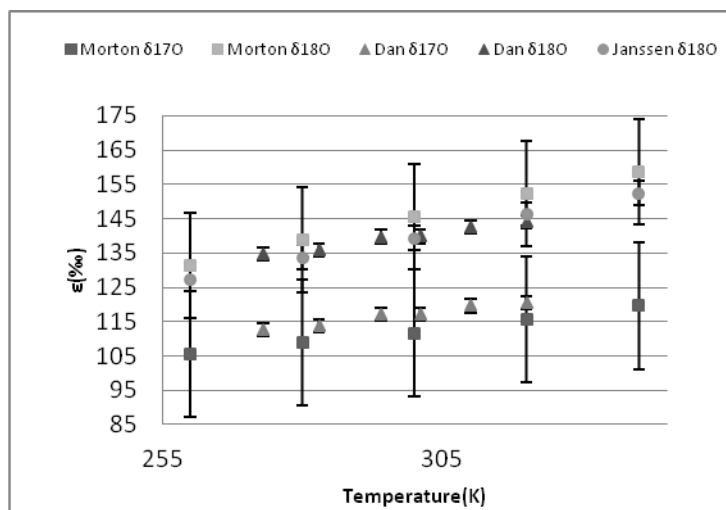


Figure 2.4: Comparison between experimental enrichments of this study (triangles), Morton (1990) (squares) and Janssen (2002) (circles). All data has been pressure corrected and $\text{O}+\text{O}_2$ depletion subtracted for direct comparison of enrichment associated with the recombination reaction.

The difference between this experiment and Morton et al. was $<4.3\text{‰}$ for $\delta^{17}\text{O}$ and $<8.6\text{‰}$ for $\delta^{18}\text{O}$ with the highest difference occurring at higher temperatures. This difference in $\delta^{17}\text{O}$ and $\delta^{18}\text{O}$ with temperature was because the $\delta^x\text{O}$ vs. temperature slopes in this experiment were smaller than those in Morton et. al.. The slope difference is likely due to the difference in experimental precision between the two studies. It is unlikely that the slope difference is associated with the shorter photolysis exposure time or different light source used as all points of comparison are within 1σ of Morton's measurements (Van Wyngarden et al., 2007).

2.4.2 Temperature and Pressure Dependence

An unanswered question concerning isotope effects during O_3 formation is whether the pressure and temperature effects are independent of each other. If they are independent, then plots of $\delta^{18}\text{O}$ (and $\delta^{17}\text{O}$) versus temperature for experiments at two different pressures should yield the same slope. The observed change in $\delta^{18}\text{O}$ values in O_3 formed between 273K and 320K at 765 torr presented here were compared to experiments that were conducted at 50 torr and 200 torr over a temperatures range of 100 to 400K (Morton et al., 1990). Morton's enrichments were nonlinear over this temperature range, but over temperatures of this experiment (273-320K), isotope enrichments were near linear (Janssen et al., 2002; Morton et al., 1990). The slopes of isotopic enhancement as a function of temperature are compared (Table 2.2).

Table 2.2: Enrichment slope as a function of temperature

	Raw Data				O+O ₂ Exchange Subtracted	
	$\delta^{17}\text{O}/\text{T}(\text{K})$	+/-	$\delta^{18}\text{O}/\text{T}(\text{K})$	+/-	$\delta^{17}\text{O}/\text{T}(\text{K})$	$\delta^{18}\text{O}/\text{T}(\text{K})$
Morton	0.235	-	0.45	-	0.174	0.339
Janssen	-	-	0.425	-	-	0.314
Experimental	0.239	0.018	0.322	0.020	0.177	0.210

The $\delta^{18}\text{O}$ versus temperature slope differed by 28% while the $\delta^{17}\text{O}$ slope only differ by 1.7%. The Morton (1990) and Janssen (2003) experiment's similar temperature dependence for $\delta^{18}\text{O}$ is not surprising given the near identical experimental setups. The significant difference in their $\delta^{18}\text{O}$ vs. temperature slopes relative to this work may be due to their lower experimental precision. Their data, approximated from Morton et. al.'s Figure 2 has a precision of $\pm 15\%$, whereas the precisions were 1.9‰ in this work. Given this large difference in precision the difference in $\delta^{18}\text{O}$ versus temperature slopes of this study may not be significantly different and when corrected for pressure (Fig 2.4).

Another possible explanation for the difference in slope is this experiment used a different light source and photolysis chamber, so photolytic isotope effects may be a factor. But this is unlikely because of the O + O₂ exchange rate would erase any isotope effect cause by O₂/O₃ photolysis. Also, the previous data was from experiments conducted in a closed reaction vessel with long photolysis times (Morton et al., 1990).

Therefore, a conclusion cannot be drawn yet about temperature and pressure codependence as our experimental conditions differ significantly from previous work.(Janssen et al., 2002;Morton et al., 1990).

2.4.3 Mass Independence and Calculation of $\Delta^{17}\text{O}$ and r_{50}

The O_3 produced in this experiment had a mass independent fractionation in agreement with other studies (Janssen et al., 2002; Mauersberger et al., 1999; Morton et al., 1990). Mass dependent fractionation is defined by the relationship between $\delta^{17}\text{O}$ and $\delta^{18}\text{O}$ measured from natural samples and varies minutely depending on the process. A mass independent fractionation (MIF) is the deviation from mass dependent enrichment that occurs during a reaction. MIF is often expressed as $\Delta^{17}\text{O}$ and is usually calculated using a simple approximation (Eq 2.10), with $\lambda = 0.52$ representing the averaged mass dependent ratio of $\delta^{17}\text{O}/\delta^{18}\text{O}$. Eq. 2.10 is an approximation of the exact logarithmic relationship (Eq 2.11), which is approximately linear over small ranges (Miller et al., 2002). Enrichment of O_3 is often considered to be mass independent, having observed $\delta^{17}\text{O}/\delta^{18}\text{O} = 1$ and thus resulting in positive $\Delta^{17}\text{O}$ values.

$$\text{Eq 2.10: } \Delta^{17}\text{O} = \delta^{17}\text{O} - (\lambda \delta^{18}\text{O})$$

$$\text{Eq 2.11: } \Delta^{17}\text{O} = 1000 \ln \left(1 + \frac{\delta^{17}\text{O}}{1000} \right) - \lambda 1000 \ln \left(1 + \frac{\delta^{18}\text{O}}{1000} \right)$$

The $\lambda = 0.52$ is an observational average and provides a reasonably accurate $\Delta^{17}\text{O}$ value but when making comparisons between studies, reaction specific λ values should be used. λ is process dependent and can range from 0.49 to 0.54 and therefore cannot be considered to be a single value. For simple reactions, such as bimolecular gas phase reactions, the λ can be approximated from a partition function calculation. For example, the O_2 exchange reaction a single average λ can be derived from the slope of the enrichments predicted from the partition function values calculated over a range of temperatures (Fig 2.5) (Miller, 2002). In complex systems that contain multiple mass

dependent oxygen fractionating reactions, such as the Chapman cycle, a reaction average λ could be applied. However, when the rates of each reaction in the cycle reconsidered, there may be one kinetically dominant reaction in which case the λ of that reaction alone can be used as λ for the approximation of $\Delta^{17}\text{O}$. In the case of the Chapman cycle, any fractionation effect arising from O_2 dissociation would be erased because the free O atom quickly undergo $\text{O} + \text{O}_2$ exchange resulting in isotopic equilibrium. Therefore, the value of λ used for all $\Delta^{17}\text{O}$ calculations in this chapter is the equilibrium exchange value of 0.5259.

Use of the proper λ is essential when comparing between data sets. Error associated with the difference in the $\text{O} + \text{O}_2$ subtracted exchange and calculation of $\Delta^{17}\text{O}$ using Eq 2.10. $\text{O} + \text{O}_2$ exchange equations from Morton (1990) and Kaye (1983) results in $\lambda = 0.5250$. A minimal difference in λ (less than 0.001) causes $\Delta^{17}\text{O}$ for ground level O_3 to deviate by $\sim 0.1\%$. This is trivial as current measurements are an order of magnitude less precise but if $\lambda = 0.52$ or Eq 2.10 are used to calculate $\Delta^{17}\text{O}$, errors exceed 2.3%. This error becomes even greater when analyzing higher enrichments of stratospheric O_3 . Therefore, by using the linear approximation rather than Equation 2.11, studies may disagree on the magnitude of the mass independent contribution when in actuality the difference may be caused from the way $\Delta^{17}\text{O}$ was calculated (Fig 2.6).

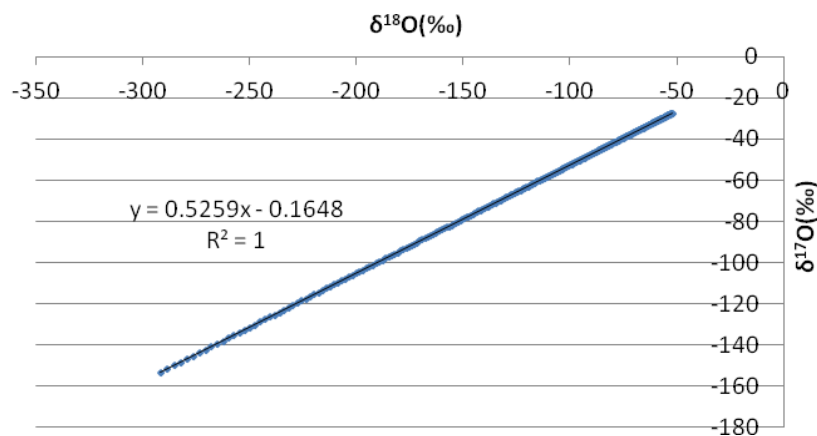


Figure 2.5: λ determination from the slope of the $O+O_2$ enrichment partition function calculation.

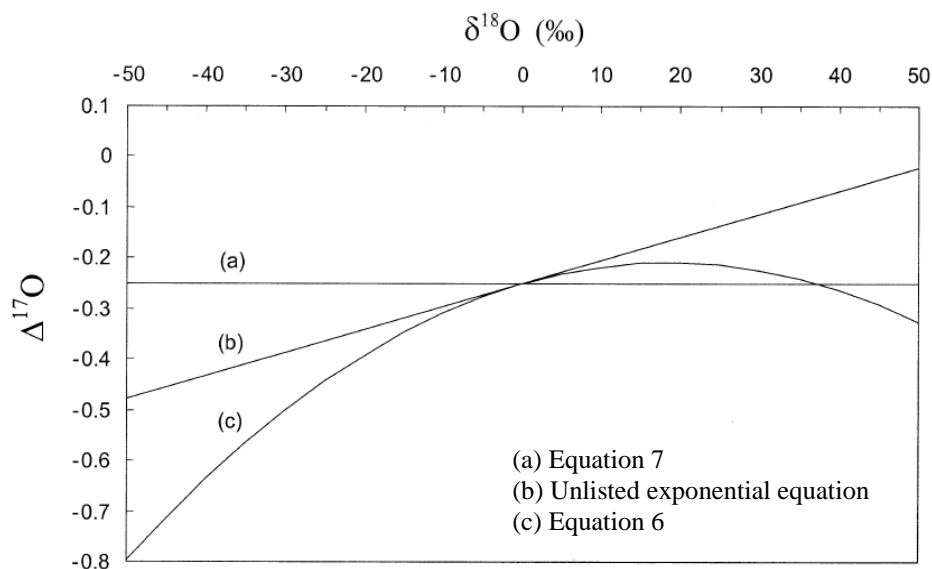


Figure 2.6: $\Delta^{17}O$ variation caused by different equation use. Adapted from Miller, 2002

This study examines the mass independent enrichment ($\Delta^{17}O$) of the experimental bulk O_3 (Table 2.1), modeled asymmetric O_3 (Table 2.5), and compares them with previous natural tropospheric O_3 data (Table 2.7). Over our experimental temperature range (273K-320K) $\Delta^{17}O$ was measured between 31.7 and 34.6‰ (Eq 2.11). Had Eq 2.10 been used, values of 33.3‰ and 36.4‰ would be expected, values well outside the 1σ

measurement. This over prediction could lead to incorrect conclusions to be drawn about O_3 enrichment and its transferred isotopic signature to other species it oxidizes. The bulk O_3 enrichment value is the basis for our modeling of asymmetric O_3 enrichment and subsequent over predictions could be as high as 2.7‰.

Bulk O_3 $\Delta^{17}O$ values are not the same as its terminal O atom because of symmetry. Isolating the asymmetric enrichment (δ^a) of the terminal oxygen and symmetric enrichment (δ^s) of the central oxygen from bulk O_3 enrichment requires a few corrections but can provide better insight into possible reaction transfer of the $\Delta^{17}O$ O_3 signature. The mass independent enrichment of O_3 is thought to primarily, if not exclusively, reside in the terminal atom (Heidenrich et al., 1986). Knowing the terminal enrichment is important for those studying NO_x and SO_2 oxidation pathways in atmospheric chemistry, as oxidation usually involves transfer of O_3 's terminal oxygen atom (Costa et al., 2011; Kunasek et al., 2010; Savarino et al., 2013; Sofen et al., 2011).

Multiple studies have shown that isotope enrichment of O_3 increases with increasing temperature and also with decreasing pressure (Janssen et al., 2003; Morton et al., 1990; S.K. Bhattacharya et al., 2002), which has been linked to isotopomer symmetry and the lifetime of the energetically excited O_3^* . As temperature increases, the greater internal energy of O_3^* will cause the lifetime before decomposition to decrease. Also, as pressure decreases, the time between collisions in the gas phase increases as average molecular distance will be greater. Therefore, if asymmetric O_3 does have a greater lifetime than symmetric O_3 (section 1.3), the effect of the proportionally longer lifetime will be greater as internal energy causes average lifetime to decrease or if frequency of

collisions to cause quenching decreases. Thus a fundamental question in theoretical models of O₃'s isotope enrichment is the role of symmetry.

Symmetry effects have been evaluated by assessing the deviation from purely statistical isotope distributions. For δ¹⁸O, the deviation from statistical distributions between the terminal and central atom of ⁵⁰O₃ is called r50, where δ¹⁸O^a and δ¹⁸O^s refer to the isotopic enrichment of the asymmetric and symmetric isotopomers of O₃ respectively (Eq 2.12) (C.Janssen, 2005). A statistical distribution of ¹⁸O would yield a r50 = 2 but , r50 > 2 is typically observed (C.Janssen, 2005). Changes in r50 values as a function of temperature have been experimentally determined using a temperature controlled reaction chamber and tunable diode laser absorption spectroscopy (TDLAS, r50 = 1.99-2.13)(C.Janssen, 2005;Larsen et al., 2000). Later studies plotted the TDLAS r50 values versus bulk O₃ δ¹⁸O values , which varies with pressure and temperature, to determine r50 from δ¹⁸O data alone (Eq 2.13)(Bhattacharya et al., 2008;C.Janssen, 2005). Over the experimental temperature range of this study's range of bulk δ¹⁸O values yielded r50 values of 2.0302 – 2.0508 (Eq 2.13). This is a deviation of less than 0.02 from the value predicted by Janssen.

$$\text{Eq 2.12: } r50 = \frac{2(1+\delta_a^{18}O)}{(1+\delta_s^{18}O)}$$

$$\text{Eq 2.13: } r50 = -2.8 \times 10^{-6} \delta^{18}O^2 + 1.932 \times 10^{-3} \delta^{18}O + 1.905$$

¹⁷O enrichment in O₃ is also expected to preferentially exist in asymmetric O₃. An r49 can be defined analogous to r50 (Eq 2.12 using δ¹⁷O). However, no spectroscopic studies of r49 have been conducted. This study does not directly measure enrichment of asymmetric O₃ directly and therefore theoretical constraints, bulk δ¹⁸O, and model

predictions were used. First, the relationship between bulk enrichment and r_{50} (Eq 2.13) was used to prediction of $\delta^{18}\text{O}^s$. $\delta^{17}\text{O}^s$ is then predicted with the assumption that $\Delta^{17}\text{O}^s = 0$ (Eq 2.11). Theoretical studies (Gao et al., 2002) and experimental work (Michalski et al., 2009) agree with this assumption asymmetric O_3 is expected to preferentially form while symmetric O_3 is seen to enrich mass dependently($\Delta^{17}\text{O}$). $\delta^{17}\text{O}^a$, and therefore $\Delta^{17}\text{O}^a$, can then be predicted using a mass balance as bulk O_3 enrichment was measured directly. Model 3 output (section 2.5.6) provided these predictions and is used to predict r_{49} .

2.4.4 Fit Model

A series of 4 models were used to evaluate the temperature dependence of O_3 isotopologue formation rates. First, an empirical “fit” model was made using a combination of Equations 2.1, 2.2, 2.8, 2.9 to yield a single equation for bulk O_3 enrichment that accounts for both pressure and temperature variation (Eq 2.14 and Eq 2.15). It should be noted that in Equation 2.14 and 2.15 it is assumed that temperature and pressure enrichment effects are independent of each other and 321K was used as the reference temperature. The observed isotopic enrichment was then used to determine α (section 2.5.5) of O_3 formation reactions once $\text{O}+\text{O}_2$ exchange depletion has been subtracted.

$$\text{Eq 2.14: } \delta^{17}\text{O} = [-8.5569(\log_{10}P)^2 + 16.803(\log_{10}P) + 105.09] + [0.2385*(T-321)]$$

$$\text{Eq 2.15: } \delta^{18}\text{O} = [-11.173(\log_{10}P)^2 + 22.456(\log_{10}P) + 116.13] + [0.3216 * (T - 321)]$$

These equations predict an isotopic enrichment that matches the experimental data for all points within 1.5‰ and can be used to predict O_3 in the atmosphere based solely on T and P conditions. However, it doesn't allow for any analysis of enrichment associated

with just the O₃ recombination rate or separation of isotopomer recombination rates. This is because experimental sample measurements are of O₃ that has also undergone fractionation from other reaction pathways, most importantly the O+O₂ exchange that was previously discussed.

2.4.5 Single IRC Models

To account for O+O₂ exchange as well as effects from other reaction pathways a photochemical box model was made using Kintecus (James C.Ianni, 2002). Kintecus is a model constructed from an MS Excel macro that uses the very small time steps and the input reactions and rate constants to calculate product and reactant concentrations over the desired model duration. With the exception of O₂ photolysis and O₃ photolysis reactions, all rates are the same as reported in Janssen(2006)(Table 4). The measured O₃ concentration from the experimental apparatus allowed for the calculation of a J₂/J₁ ratio using the steady state approximation. This ratio was calculated to be 72,000/1 indicating the rate of O₃ photolysis is much greater than that of O₂ photolysis. This was expected since the primary output of the UV source used was near O₃ peak absorptions at 254nm. J₂ was calculated using the known output from the Hg vapor lamp and J₁ was determined using the J₂/J₁ ratio. Double and triple substituted O₃ isotopologue formation reactions were not considered because they are produced at <10⁶ molecules/cm³ and would result in a negligible difference in predicted O₃ enrichment (<0.1‰).

Model 1 uses single O₃ isotopomer rate coefficients (IRC) for ¹⁷O and ¹⁸O (R2.5-R2.10)(Table 2.3), i.e. the XOO and OXO rate coefficients are the same (X=¹⁷O, or ¹⁸O). The IRC was calculated by subtracting O+O₂ exchange (Eq 2.6, 2.7) from enrichments

using Eq 2.14 and 2.15 to yield a single α (Eq 2.16, 2.17). The IRC represents isotopic fractionation factor (α) for each reaction pathway and is related to isotopic enrichment by $\delta^x\text{O}=(\alpha^x-1)*1000$.

$$\text{Eq 2.16: Model 1 } ^{49}\text{O}_3\text{IRC} = \frac{[\delta^{17}\text{O} - ((\alpha^{49}\text{O}_3 - 1) * 1000)]}{1000} + 1$$

$$\text{Eq 2.17: Model 1 } ^{50}\text{O}_3\text{IRC} = \frac{[\delta^{18}\text{O} - ((\alpha^{50}\text{O}_3 - 1) * 1000)]}{1000} + 1$$

The model results are in good agreement with the experimental observations. The model runs was run for 2 seconds, which is the residence time of the gas in the photolysis chamber. The model achieves isotopic equilibrium (<0.1‰ variability) in ~0.1s. It also predicts an O₃ concentration that agreed with the experimentally measured values, to within 8%. Over the experimental temperature range, the model predicted $\delta^{18}\text{O}$ and $\delta^{17}\text{O}$ values within 3‰ of the experimental values. Model 1 was only intended to predict bulk O₃ isotopic enrichment and not differentiate IRCs. Observational and theoretical concerns suggest that O₃ IRCs are different, and this was addressed in Model 2.

Table 2.3: Photochemical box model reactions and rates

Rxn	Reaction	Rate Coefficient [IRC]
R2.3	$O_2 \rightarrow O + O$	$j_1 = 1.204 \times 10^{-5}$
R2.4	$O + O_2 + M \rightarrow O_3 + M$	$k_1 = 6.0 \times 10^{-34} * (300/T(K))^{2.5}$
R2.5	$O + OP + M \rightarrow OOP + M$	$k_2 = IRC * k_1$
R2.6	$O + OP + M \rightarrow OPO + M$	$k_3 = IRC * k_1$
R2.7	$P + O_2 + M \rightarrow OOP + M$	$k_4 = IRC * k_1$
R2.8	$O + OQ + M \rightarrow OOQ + M$	$k_5 = IRC * k_1$
R2.9	$O + OQ + M \rightarrow OQO + M$	$k_6 = IRC * k_1$
R2.10	$Q + O_2 + M \rightarrow OOQ + M$	$k_7 = IRC * k_1$
R2.11	$O_3 \rightarrow O + O_2$	$j_2 = 8.671 \times 10^{-1}$
R2.12	$O + O_3 \rightarrow 2O_2$	$k_8 = 8.0 \times 10^{-12} * e^{(-2060/T(K))}$
R2.13	$P + O_2 \rightarrow O + OP$	$k_9 = k_{11} * 0.5259$
R2.2	$O + OP \rightarrow P + O_2$	$k_{10} = k_9 / K_2$
R2.14	$Q + O_2 \rightarrow O + OQ$	$k_{11} = 1.27 * e^{(50 * ((1/T(K)) - (1/300)))} * k_{13}$
R2.1	$O + OQ \rightarrow Q + O_2$	$k_{12} = k_{11} / K_1$
		$k_{13} = 4.42 \times 10^{21} * (300/T(K))^{-1.58} * k_1$
		$K_1 = 1.9456 * e^{(31.782/T(K))} * (1 - (9.3 \times 10^{-6} * T(K)) + (1.97 \times 10^{-8} * T(K)^2))$
		$K_2 = 2 * ((0.5259 * ((K_1/2) - 1)) + 1)$

Model 2 defined unique IRCs for both ^{18}O and ^{17}O isotopomers. IRCs for both Q+OO (R2.10) and O+OQ (R2.8, R2.9), where Q = ^{18}O were defined for the O_3 recombination reactions, analogous P (^{17}O) isotopomers were defined for ^{17}O (R2.7 and R2.5, R2.6). The O_3 formation IRCs were initially set to the values from Mauersberger(1999) and Janssen(2002) respectively. Model 2 used the same IRCs for asymmetric and symmetric products in the O+OQ (R2.8, R2.9) and O+OP (R2.5, R2.6) reactions. These average IRCs have a small temperature dependence as reported by Janssen(2002). The IRCs in Model 1 used linear temperature dependence for each pathway but previous work has shown that the IRC temperature dependence is almost entirely in the Q+OO and P+OO formation pathways(Janssen et al., 2002).

Initial Model 2 output yielded $\delta^{18}\text{O}$ predictions that were within 2.9‰ of all experimental values, but it predicted a greater $\delta^{18}\text{O}$ temperature dependence (0.4257‰/T(K)) relative to what was observed (0.322‰/T(K)). When the temperature dependence of IRC R2.10 was altered to reflect this study's experimental slope, all model $\delta^{18}\text{O}$ values were within 1.6‰ and output $\delta^{18}\text{O}$ temperature dependence was within 0.019‰/T(K) of the experimental value. When Mauersberger's (1999) values for P containing O_3 formation reactions are applied there is a 6‰ over prediction for $\delta^{17}\text{O}$ but this was resolved by changing the R2.5 and R2.6 IRC from 1.17 to 1.16. This is an alteration well within 1σ of Mauersberger's values and allowed for agreement with experimental data within 1.5‰.

2.4.6 Split Pathway IRC Model

The objective of Model 3 is to use the experimental $\delta^x\text{O}$ data and r50 values to determine separate asymmetric and symmetric IRCs to predict asymmetric and symmetric isotopomer enrichment. This could be used in future work involving O_3 interaction with other atmospheric species to better predict the transferred oxygen enrichment via those reaction pathways. The IRC for R2.7 and R2.10 were not changed (Model 2) but the O+OQ (R2.8, R2.9) and O+OP (R2.5, R2.6) reactions were given a separate IRC for the symmetric and asymmetric pathway. Janssen's (1999) rates were used as a starting point and compared with the expected r50 calculated using experimental $\delta^{18}\text{O}$ values and Eq 2.13. This r50 of 2.137 resulted in elevated bulk and terminal enrichment of 94.1 ‰ and 118.3‰ respectively, which is an over prediction of r50 by 0.096 and bulk enrichment by 13.3‰. While the over prediction of r50 may seem

minor, it would result in an over prediction of terminal ^{18}O enrichment by 28.9‰. The two pathways were updated to reflect Janssen's(2002) joint IRC for the O+OQ (R2.8, R2.9) reaction (1.246) and adjusted to match the expected r50. The values used (Table 2.4) agreed with the expected r50 and predicted bulk ^{18}O enrichment that was within 1.7‰ of the observations.

The ^{18}O IRCs are well documented (Gao et al., 2002;Janssen et al., 2001;Janssen et al., 2002;Mauersberger et al., 1999), but r49 and IRC values for the two O+OP (R2.5, R2.6) pathways are lacking. Without a defined r49 starting point, $\Delta^{17}\text{O}_s=0$ was assumed as all mass independent enrichment is expected to reside in asymmetric O_3 . With the ^{18}O IRCs set to match the predicted r50, the symmetric ^{17}O was adjusted to match the $\Delta^{17}\text{O}_s=0$ assumption. Then, the asymmetric ^{17}O IRC was calculated from the average O+OP (R2.5, R2.6) IRCs used in Model 2. The resulting model asymmetric and symmetric $^{49}\text{O}_3$ enrichments were used in Eq 2.12 to calculate r49. The predicted r49 (Table 2.5) demonstrate results similar to that of Bhattacharya(2008), where r49 is seen to be larger than r50 and allow for agreement of ^{17}O enrichment within 1.5‰.

Table 2.4: Applied IRC values for all isotopically substituted O_3 formation reactions for this study's models as well as previous works (@300K)

Reaction	Model 1	Model 2	Model 3	Mauersberger 1999	Janssen 2005	Janssen 1999
O+OP → OOP	1.117	1.16	1.2590	1.17	-	-
O+OP → OPO	1.117	1.16	1.0610	1.17	-	-
P+OO → OOP	1.117	1.03	1.03	1.03	-	-
O+OQ → OOQ	1.146	1.246	1.3913	1.27	1.246	1.45
O+OQ → OQO	1.146	1.246	1.1007	1.27	1.246	1.08
Q+OO → OOQ	1.146	0.92	0.92	0.93	0.92	0.92

Table 2.5: Predicted enrichment and symmetry ratios from Model 3

T(K)	r49	δ^{17a}	δ^{17s}	r50	δ^{18a}	δ^{18s}	Δ^{17O^a}
270	2.1087	89.03	32.41	2.0289	78.53	62.46	45.2
280	2.1138	92.30	33.31	2.0338	82.24	64.36	46.4
290	2.1189	96.20	33.63	2.0387	87.02	64.88	47.5
300	2.1238	98.32	34.47	2.0435	89.37	66.52	48.6
310	2.1287	101.42	34.76	2.0482	93.05	67.20	49.8
320	2.1336	104.52	35.65	2.0529	96.60	68.89	50.9

The predicted asymmetric enrichment can then be used with Eq 2.11 to arrive at Δ^{17O^a} .

This mass independent enrichment is transferrable to subsequent species O_3 interacts with and can result in enrichments greater than that of bulk O_3 (McCabe et al., 2007). For an approximation without using the photochemical box model, Equations 2.15, 2.13, and 2.18 can be used to approximate Δ^{17O^a} from temperature and pressure. Also, Equations 2.14, 2.19 and 2.20 can be used for approximating the IRC of the split O+OP (R2.5, R2.6) pathways while Equations 2.15, 2.21 and 2.22 can be used for the split O+OQ (R2.8, R2.9) pathways.

$$\text{Eq 2.18: } \Delta^{17O^a} = 238.144 * r50 - 439.977$$

$$\text{Eq 2.19: } O + OP \rightarrow OOP \text{ IRC} = -1.833 \times 10^{-4} * \delta^{17O} + 1.2734$$

$$\text{Eq 2.20: } O + OP \rightarrow OPO \text{ IRC} = 1.833 \times 10^{-4} * \delta^{17O} + 1.0466$$

$$\text{Eq 2.21: } O + OQ \rightarrow OOQ \text{ IRC} = -3.317 \times 10^{-4} * \delta^{18O} + 1.4185$$

$$\text{Eq 2.22: } O + OQ \rightarrow OQO \text{ IRC} = 3.317 \times 10^{-4} * \delta^{18O} + 1.0735$$

With the expectation that asymmetric O_3 is the source of mass independent enrichment due to its longer lifetime, it would be expected that with constant pressure and increasing temperature that the asymmetric (R2.5, R2.8) IRC would increase. However, this is not the case and the IRC can be seen as near constant but with a slight inverse relationship to

temperature. This could be due to several causes based on the precision of previous spectroscopic work. While the temperature dependence of formation is expected to lie almost exclusively within R2.10, there may be some contribution from R2.8 and R2.9 within that observed rate. Also, if there were a slightly larger temperature dependence within the O+OQ reaction (R2.8, R2.9), which would likely reside in the asymmetric production pathway, then the change in the IRC with temperature would likely show the expected trend. As this study only took measurements of bulk O₃ enrichment, direct inference as to the specific reason for the discrepancy cannot be determined.

2.4.7 Model Isotopic Enrichment Predictions

O₃'s $\delta^{17}\text{O}$, $\delta^{18}\text{O}$, and $\Delta^{17}\text{O}$ values produced by various temperature and pressure conditions were predicted using the fit model and 3 photochemical box models. The fit model showed how $\delta^{18}\text{O}$ and $\delta^{17}\text{O}$ values vary with pressure dependence and this experiment's temperature dependence. Predicted bulk O₃ isotopic enrichment based only on temperature and pressure dependent isotopic enrichment (Table 2.6) differed by less than 1‰ on average for both $\delta^{17}\text{O}$ and $\delta^{18}\text{O}$ and never more than 1.5‰ for any point. Model 1, a box model with homogenous rate coefficients for O₃ formation reactions, resulted in values within 3‰ of experimental values (James C. Ianni, 2002). Model 2, which separated IRCs for both O+OQ (R2.8, R2.9) and O+OP (R2.5, R2.6) O₃ formation pathways, better predicted bulk enrichment values and differed from experimental values by less than 1.6‰ for all points. Model 3 allowed for prediction of bulk enrichment (within 1.7‰) and asymmetric/symmetric O₃ enrichment individually. Models 2 & 3 offered similarly accurate predictions of bulk O₃ enrichment with an average deviation

from experimental values less than 1‰. Making predictions of greater accuracy would require greater experimental precision as our model predictions were as precise as our experimental data ($\pm\sim 1\%$).

Table 2.6: Model output and deviation from experimental data for isotopic enrichment of O_3 .

T(K)	Experimental		Fit Model				Model 1				Model 2				Model 3			
	$\delta^{17}O$	$\delta^{18}O$	$\delta^{17}O$	+/-	$\delta^{18}O$	+/-	$\delta^{17}O$	+/-	$\delta^{18}O$	+/-	$\delta^{17}O$	+/-	$\delta^{18}O$	+/-	$\delta^{17}O$	+/-	$\delta^{18}O$	+/-
273	70.8	72.4	71.2	0.4	72.9	0.5	69.5	-1.3	70.1	-2.3	70.1	-0.8	73.1	0.7	70.2	-0.7	73.2	0.8
283	72.6	74.6	73.6	1.0	76.1	1.5	72.0	-0.7	73.3	-1.3	72.6	-0.1	76.2	1.6	72.7	0.0	76.3	1.7
294	76.8	80.0	76.2	-0.6	79.7	-0.3	74.6	-2.2	76.9	-3.0	75.3	-1.5	79.6	-0.4	75.3	-1.5	79.7	-0.3
301	77.3	80.8	77.9	0.6	81.9	1.1	76.3	-1.0	79.2	-1.6	77.0	-0.4	81.7	0.9	77.0	-0.3	81.8	1.0
310	80.1	84.6	80.0	-0.1	84.8	0.2	78.5	-1.6	82.1	-2.5	79.1	-1.0	84.4	-0.2	79.2	-0.9	84.4	-0.2
320	81.6	87.0	82.4	0.9	88.0	1.1	80.9	-0.6	85.4	-1.5	81.5	-0.1	87.3	0.4	81.6	0.0	87.4	0.4

2.5 Comparison with Atmospheric Measurements

Previous studies have attempted to directly collect and analyze tropospheric O_3 for its stable isotope composition (Johnston et al., 1997; William C. Vicars et al., 2012)(Table 2.7). Using the direct sampling method, Johnston(1997) observed tropospheric O_3 $\delta^{18}O$ and $\Delta^{17}O$ values similar values to our experimental results (Table 2.7). The sampling locations, all in the southwestern US, had very different environments as Pasadena and La Jolla are populated urban environments while White Sands Missile Range (WSMR) is in a fairly remote region and at a greater elevation (5000ft). The mean temperature at the three locations sampled by Johnston (1997) (Weather Underground, 2013) was used with Model 3 to predict the O_3 $\delta^{17}O$, $\delta^{18}O$ and $\Delta^{17}O$ values. There is relatively good agreement between the fit data and the mean values from all 3 locations. The mean $\Delta^{17}O^a$ prediction from each location was within 7‰ of the prediction of Model

3. This demonstrates successful model predictions given the wide range of measured $\Delta^{17}\text{O}$ values (17.9-39.4) and the limitations of the cryogenic trapping apparatus used to collect early tropospheric O_3 . $\Delta^{17}\text{O}^a$ predictions from Vicars et. al. are not altered to directly compare with model 3 as their work used a $3/2 \Delta^{17}\text{O}^a/\Delta^{17}\text{O}$ ratio for precision of asymmetric enrichment but is still shown for comparison. The comparison between laboratory and natural data would be ideal when remote locations are considered as sample contamination and system complexity are limited. For that reason, WSMR is likely the best comparison and is seen to be in the best agreement with our predictions ($\Delta^{17}\text{O}^a$ deviation of 4.2%).

Table 2.7: Average tropospheric O_3 data and predicted asymmetric enrichment compared with Model 3 prediction (Johnston et al., 1997; William C. Vicars et al., 2012).

Location(n)	T(K)	$\Delta^{17}\text{O}^a$	$\Delta^{17}\text{O}^a$	$\Delta^{17}\text{O}^a$	$\sigma(\Delta^{17}\text{O}^a)$
		Max	Min	Avg	
La Jolla, CA(29)	290.3	46.2	35.7	40.5	2.5
White Sands Missile Range, NM(6)	286.3	45.6	41.4	43.3	1.6
Pasadena(7)	296.0	44.0	38.8	42.0	2.1
Experimental(Fit Data)	290.0	--	--	47.5	--
Grenoble, France(20)	286.0	38.7	29.2	34.3	2.9

2.5.1 Predicted O_3 $\Delta^{17}\text{O}$ Enrichment as a Function of Altitude

With an experimentally validated model that can predict the isotopic enrichment of O_3 as a function of temperature and pressure, O_3 enrichment values can be modeled as a function of altitude. Assuming a dry adiabatic lapse rate 9.7K/km and a scale height of 8.7km, Fig 2.8 shows the expected $\Delta^{17}\text{O}^a$ trend with increasing altitude (28-35km). The temperatures are outside the temperature range of this study and therefore the enrichment trend is extrapolated but is still shown for comparison (C. David et al., 2012). There are

many factors to consider when analyzing various atmospheric species (NO_x , SO_x) as they undergo many reactions other than O_3 oxidation. However, the presence of a mass independent isotopic signature ($\Delta^{17}\text{O} > 0$) comes almost exclusively from direct interaction with O_3 and can be used to trace O_3 's role in the atmosphere. Isotopic enrichment of asymmetric O_3 must be accurately predicted in order to quantify how much O_3 interaction has taken place and our work suggests that $\Delta^{17}\text{O}^a \approx 47.5\text{‰}$ is a valid approximation for average enrichment from O_3 formation at ground level conditions.

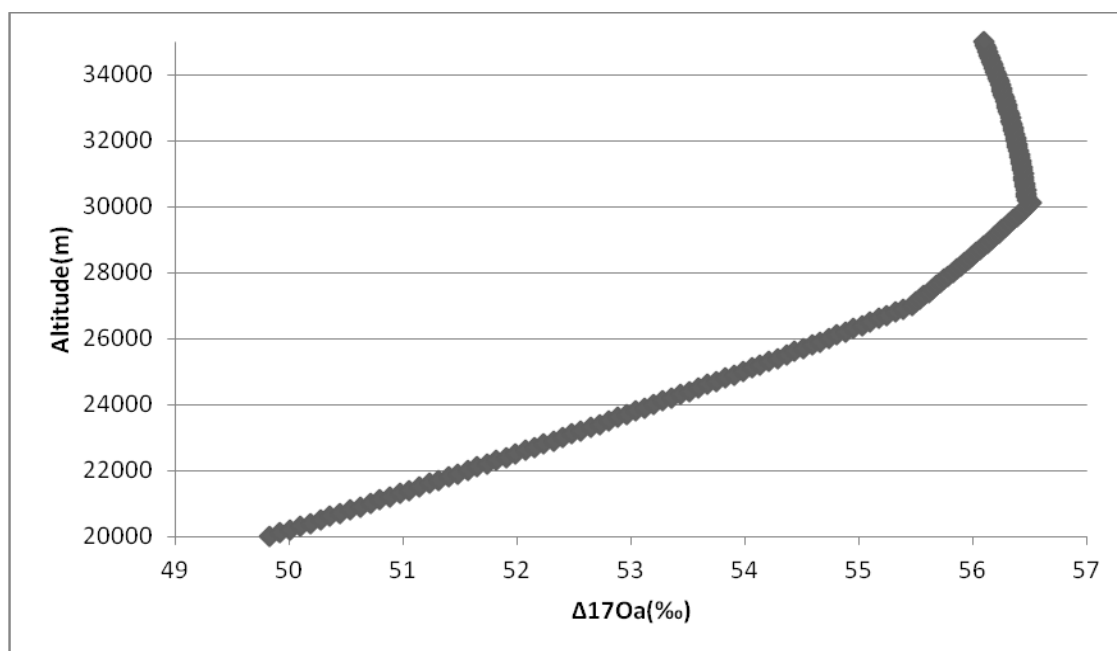


Figure 2.7: Predicted $\Delta^{17}\text{O}^a$ change with altitude(stratosphere).

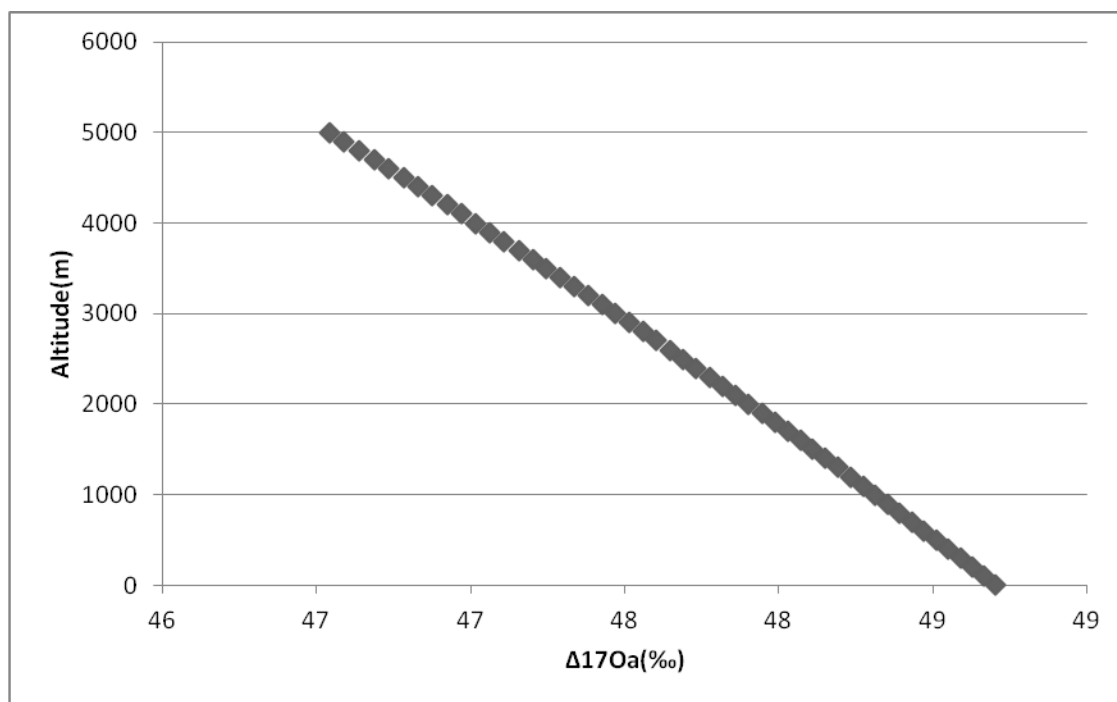


Figure 2.8: Predicted $\Delta^{17}\text{O}^a$ change with altitude (troposphere).

2.6 Conclusions and Limitations

Understanding O_3 formation enrichment is an ongoing process and while the nature of enrichment has yet to be completely explained, there has been significant progress made in narrowing the potential errors associated with temperature dependency. The experiments performed provided a great deal of information on temperature dependent enrichment in an open flow, photolysis system. Despite measured enrichments being only representative of the bulk O_3 , it is still possible to make a good approximation of the asymmetric enrichment. Building on the previous work of Janssen(2003, 2005) and Morton (1990), enrichments of the flow system are seen to be within a similar range of total enrichment and error has been reduced from 13% of enrichment magnitude down to 3% at 1σ . As the aim of this work was to focus on tropospheric conditions, 273 – 320K

was examined and in that range temperature dependent enrichment can be expressed linearly.

The use of photochemical box modeling allowed for approximation of isotopologue rate coefficients for all O₃ formation pathways with minimal assumptions from previous works (Janssen et al., 2002; Mauersberger et al., 1999). While there may be precision related issues with the ability to separate each pathway, bulk enrichment output showed agreement with experimental values within 1.7‰. When combined with the work of Janssen (2005) and Bhattacharya (2008), asymmetric enrichment resulting in a mass independent enrichment signature ($\Delta^{17}\text{O}^a \approx 47.5\text{‰}$) can be approximated.

The ability to approximate terminal enrichment of oxygen in O₃ also provides insight into how reaction pathways could be examined using $\Delta^{17}\text{O}$ as a tracer for interaction with O₃. Vicars (2012) has already examined isotope transfer from O₃ to nitrite in solution to form nitrate, which may be considered analogous to a variety of O₃ interactions with NO_x species. When compared with tropospheric data from Vicars (2012) and Johnston (1997), there is reasonable agreement that is likely limited due to other contaminating factors at sample locations. The most remote location (WSMR) was in great agreement with the data presented and while complex urban environments may be currently beyond the scope of direct comparison, there is potential to gain perspective on why sampling in those locations differs.

CHAPTER 3. A PROXY METHOD FOR SAMPLING ISOTOPES OF O₃

3.1 Introduction

O₃ is an important oxidant in tropospheric reactions and its unique isotopic signature can be used as a tracer to better understand those reactions, but this requires knowing the isotopic composition of tropospheric O₃. Most oxygen containing molecules are fractionated mass dependently, meaning their $\delta^{17}\text{O}/\delta^{18}\text{O}$ ratio is ~ 0.52 . O₃ fractionates mass independently and often has a $\delta^{17}\text{O}/\delta^{18}\text{O}$ ratio > 0.8 . Any deviation from the mass dependent ratio is calculated as $\Delta^{17}\text{O}$ (section 1.4). As O₃ reacts with other molecules in the atmosphere any transferred oxygen atom from O₃ to the product molecule will cause a $\Delta^{17}\text{O} > 0$. This can potentially be used to describe the reaction mechanism and how great a role O₃ has played.

Laboratory studies have been performed to investigate O₃'s large isotopic enrichments. Primarily the focus has been on what causes these isotopic enrichments and how are they affected by temperature and pressure. This thesis along with previous laboratory studies all show that both pressure and temperature have a significant affect as isotopic enrichment increases with increasing temperature and decreasing pressure. But it is unclear whether the isotope effects in O₃ produced in well controlled lab studies is the same as that in the troposphere where it undergoes significant secondary reactions and is produced by NO_x rather than O₂ photolysis.

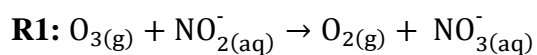
O₃ in the troposphere is difficult to directly collect for isotope analysis. This because its mixing ratios are ~10 ppb_v in pristine environments to ~50 ppb_v in polluted environments. The current method collects and purifies tropospheric O₃ using a complex set of reactive and cryogenic traps that are difficult to operate, expensive and requires 10+ hrs of sampling time (Johnston et al., 1997). The accuracy and precision of this method is also questionable. For example, if the traps or system pressure were to change significantly during O₃ collection, condensed O₃ could reenter the gas phase which would likely result in retention of isotopically heavy O₃ as the lighter isotopologue would preferentially degas. Therefore, a new accurate, efficient and cost effective way of collecting tropospheric O₃ for isotopic analysis would be highly desirable. .

This chapter discusses an attempt to develop a proxy approach to analyzing the isotope composition of tropospheric O₃. The proxy approach would use O₃ to oxidize another compound and the oxygen isotope composition of the reaction product would be analyzed as a surrogate for O₃. The requirements for the proxy approach are that 1) O₃ must quantitatively and easily transfer one or more of its O atoms to the product compound 2) The reaction product must not readily undergo isotopic exchange with its surroundings and 3) analysis of the product is relatively straightforward. Nitrite was chosen as the proxy reactant because it reacts with O₃ very efficiently to form nitrate and this reaction meets the three proxy method criteria. The O₃+ NO₂⁻ reactivity, atom transfer, and the isotope exchange properties of the reaction are detailed in section 3.2. An experimental bubble chamber to facilitate the gas (O₃) to aqueous (NO₂⁻) reaction was built and tested and is discussed in 3.3. Discussions of analysis issues caused by analytical blanks, methods of purifying the NO₂⁻ reagent, and approaches to removing

excess NO₂⁻ post reaction are discussed in sections 3.4, 3.5, and 3.6 respectively. Details of the isotope analysis of the product NO₃⁻ using two different established methods are discussed in section 3.7.

3.2 O₃/NO₂⁻ Reactivity and Isotope Transfer

Measuring O₃'s isotopic enrichment by proxy directly requires rapid and quantitative transfer of an O atom to a product molecule. NO₂⁻ reacting with O₃ to produce NO₃⁻ in an aqueous solution meets these requirements. The rate of O₃ + NO₂⁻ → NO₃⁻ + O₂ (5.83 × 10⁵ M⁻¹s⁻¹, R1) reaction is rapid (Liu et al., 2001), therefore an apparatus which can facilitate the transport of gas phase O₃ into a solution of NO₂⁻ should quantitatively produce NO₃⁻. Dynamical calculations show that the reaction occurs through the abstraction of the terminal O₃ atom (Liu et al., 2001). There is interest in the isotopic variation of the terminal atom of O₃ because it can test symmetry effects postulated by theory so the reaction is also ideal in that respect (section 3.5.3). It has been shown that quantitative of O₃ terminal atom transfer does occur and that the isotopes are conserved during the reaction (Michalski et al., 2009). Also the product NO₃⁻ does not undergo isotopic exchange with water at pH > 4 (Bunton et al., 1952; C.A. Bunton et al., 1953), thus it would preserve the isotope transfer during storage (see further discussion in section 3.6). Therefore, if a sampling method using this reaction could be proven to be effective, this could be a new accurate, efficient and cost effective way of determining tropospheric O₃ for isotopic composition.



3.3 Ozone Scrubbing Method Using a NO₂⁻ Bubbler

An experimental bubble chamber to facilitate the gas (O₃) to aqueous (O₃) transfer and subsequent O₃ + NO₂ reaction was built and tested (Fig 3.1). Gas bubblers were chosen that had a fritted disk with a fine pore size and large surface area to maximize flow while maintaining fine bubble size. The initial O₃ concentration was determined using a 2B Technologies O₃ monitor that monitor took 10s averages of O₃ concentration placed prior to the bubbler containing an NO₂⁻ solution. The NO₃⁻ yield was calculated by the product of the average O₃ concentration (ppb_v), number density of atmospheric gas(molecules/cm³), flow rate(cm³/s), sampling time(s), and scrubbing efficiency divided by Avagadro's number(N_A)(Eq 3.1).

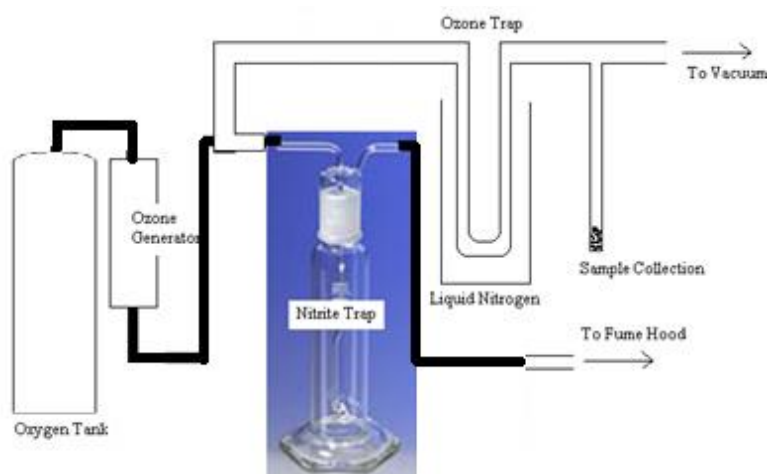


Figure 3.1: Laboratory O₃ bubbler apparatus

$$\text{Eq 3.1: } \text{NO}_3^- (\text{mol}) = \frac{[\text{O}_3] * 2.7 \times 10^{19} * 25 * t * 0.99}{N_A}$$

The rate at which gas phase O₃ molecules will diffuse within the bubble and either contact the solution at the bubbles surface or be absorbed into solution and react with NO₂⁻ depends on the bubble size. If the gas flow rate through the bubbler is constant the

bubbles should have a uniform bubble size distribution and will take the same time to exit the solution based on solution depth. Since O_3 must diffuse to the bubbles surface to react, the smaller the bubble size the shorter the diffusion distance and thus the more efficient the reaction. Small bubble size was maintained by regulating flow with an Omega flow meter and using a fritted disc with the finest pore size that doesn't limit gas flow. Experiments showed that a < 2 second bubble transit time was sufficient for $\sim 99\%$ of the O_3 to be removed (Fig 3.2).

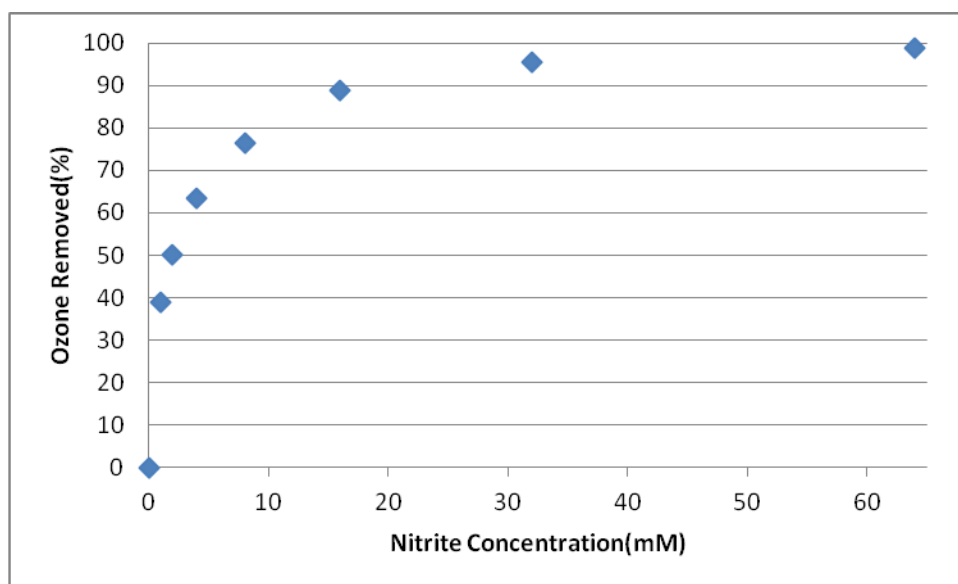


Figure 3.2: O_3 scrubbing efficiency with NO_2^- concentration

High O_3 scrubbing efficiency was found to be a function of the NO_2^- concentration. Trials were conducted to assess what NO_2^- concentration would be the ideal scrubbing solution. Small bubble size were critical and the sizes were qualitatively assessed through side by side digital image comparison and were found to decrease with increasing salt concentration. Bubble size increased with increasing flow rate so flow rate

was limited to 1.5 L/min as bubbles were sufficiently small to maintain 99% reaction efficiency. NO_2^- was chosen because it reacts with O_3 and decreases bubble size. NO_2^- concentrations were tested from 1mM to 1M and bubble size was seen to decrease with increasing concentration (Fig 3.2). At 64mM, the NO_2^- solution removed 99% of all O_3 and above that concentration scrubbing efficiency increased minimally (< 0.5% increase at 128mM). The higher NO_2^- concentration without increasing the product yield is not advantageous because excess NO_2^- would need to be removed in later processing steps. High scrubbing efficiency is desirable because this would improve the temporal resolution of real world O_3 sampling. Also, while other trace oxidant species could react with the NO_2^- solution, they exist in such low concentrations that they will not affect later isotopic measurements. Despite the abundance of molecular oxygen (O_2), it will not react with NO_2^- and therefore will not affect isotopic analysis of O_3 but the solution is light sensitive and must remain covered whenever possible (Mack, 1999).

For the NO_2^- proxy methods to be considered an effective means of determining tropospheric O_3 's isotopic composition, laboratory measurements of the product NO_3^- must be proportional to the O_3 it was reacted with. Laboratory O_3 reactions were done to compare isotopic enrichment of the product NO_3^- and collected bulk O_3 . A high purity oxygen tank (99.99%) was connected to an O_3 generator (Prozone) which produced O_3 concentrations in excess of 100ppm_v and simultaneously bubbled through the 64mM NO_2^- solution and collected in a vacuum line system. The vacuum line O_3 was then condensed onto a sieve trap which converted it to O_2 which is then analyzed using the dual inlet IRMS. The NO_2^- solution, now containing significant NO_3^- (>1mmol), had excess NO_2^- removed through reaction with azide (see section 3.6.1). The acidic NO_3^-

solution was then neutralized and converted to AgNO_3 salt that is thermally decomposed to O_2 and again isotopically analyzed using the dual inlet IRMS. The O_3 was collected directly in cryo traps (section 3.3) and the resulting O_2 gas was analyzed on the dual inlet IRMS.

Since the terminal atom of O_3 that reacts with NO_2^- to form NO_3^- is expected to have a $\Delta^{17}\text{O}$ 1.5 times greater than bulk O_3 value (see Chapter 2). Since the extracted O atom account for only 1 of 3 in the NO_3^- molecule, the other from the NO_2^- reactant, $\Delta^{17}\text{O}$ of NO_3^- should be $\frac{1}{2}$ of the measured bulk O_3 value $\Delta^{17}\text{O}$. NO_3^- from these few tests had varied $\Delta^{17}\text{O}$ values due to unrefined NO_2^- solution processing but values of $\sim 12\text{‰}$ were common. The data was sparse and of low precision but it does lead to an expected $\Delta^{17}\text{O}$ of the reacted O_3 of 24‰. This is below $\Delta^{17}\text{O}$ O_3 values measured in later work ($\sim 30\text{‰}$, section 2.3). While this does not prove that O_3 $\Delta^{17}\text{O}$ quantitation was possible, it does demonstrate the validity of the bubbler sampling method as any NO_3^- not produced from reaction with O_3 would have a $\Delta^{17}\text{O} = 0$.

3.4 NO_3^- Contaminant in NO_2^- - Bubbler Solutions

It is important that all NO_3^- in the solution was generated from NO_2^- reacting with O_3 , rather than being a reagent blank. The initial NO_2^- solutions were made from KNO_2 salts (98%+). A small amount of NO_3^- impurity ($>10\mu\text{mol}$ in 12.8mmol of NO_2^-) was always present in the solutions. Since NO_2^- solutions were made in bulk and stored for later use the source of the NO_3^- contaminant may have been NO_3^- production during storage. NO_3^- contaminant quantity in NO_2^- solutions can be affected by solution pH as well as the container they're being stored in generating NO_3^- at a slow but non negligible rate(Jean-

Claude Wolff et al., 1997). Solutions were also made just prior to use but the NO_3^- blank persisted which means it is likely a salt impurity. This is problematic since blank NO_3^- will have a $\Delta^{17}\text{O}=0$ which causes dilution of the measured $\Delta^{17}\text{O}$ value yielding a measurement between 0 and that of the $\Delta^{17}\text{O}$ of O_3 reacted NO_3^- . If the contaminant amount were consistent then it could be calibrated for and accurate measurements related to $\Delta^{17}\text{O}$ of O_3 could be calculated.

3.5 Eliminating NO_3^- Contaminant from the NO_2^- Solution

3.5.1 Eliminating NO_3^- Contaminant from the NO_2^- Solution by Chromatography

The NO_2^- solution purity can be improved using anion exchange resin. These resins separate anions based on their binding affinity and can be used to separate NO_3^- from NO_2^- . An anion exchange resin was chosen because the anion capacity (the amount of anions retained on the column) can be easily varied by adjusting the resin quantity used. Also, post separation collections of NO_3^- are simpler than with traditional HPLC because it's a non-destructive separation method and has higher eluent flow rate. Anion binding efficiency describes the ability of any ion to bind to the resin preferentially over other anions. NO_3^- and NO_2^- , however, have very similar binding efficiencies which makes them difficult to separate because of the large amount of NO_2^- present. Ideally, resin separations are performed by having enough resin to trap the anion with higher trapping efficiency while the other anion(s) flow freely through the column for collection or disposal. To improve separation characteristics the resin's anionic "form" was changed. Anionic form refers to the anion that is bound to the resin before separation is attempted.

The form can be changed by treating resin with a concentrated solution of the anion you'd like to change it to. We chose to change resin to OH^- form after chloride separations proved ineffective. Hydroxyl form was chosen because of its low binding efficiency which meant it would be easily displaced by NO_3^- or NO_2^- and potentially allow for better separation.

Changing column length, eluent concentration, and eluent flow rate were also unsuccessful at completely separating NO_3^- from NO_2^- . When column selectivity is insufficient to separate anions, rate of separation must be slowed to improve column resolution. This can be done by using more resin in a longer column to allow NO_3^- and NO_2^- more substrate to interact with thereby allowing them to separate more effectively. This was not an ideal choice due to the high cost of resin as well as the long resin regeneration process which generated significant waste that must also be processed. Another way to slow separation is to change eluent concentration and flow rate. Eluent is the solution used to displace the NO_3^- and NO_2^- from the resin and move them down the column for collection. The anion chosen for the eluent must have a high enough binding efficiency to displace the analyte but not so high as to not allow it to rebind. By lowering analyte concentration or slowing eluent flow rate, a shorter column can be used but separation times become longer. Neither method was successful in completely separating NO_3^- from NO_2^- and while it may have been possible with optimized column and eluent conditions, those conditions would be prohibitively expensive so a different NO_2^- purification process was needed.

3.5.2 Eliminating NO_3^- Contaminant from the NO_2^- Solution by Cadmium Reduction

An alternative approach is to reduce the NO_3^- contaminant to NO_2^- using Cadmium (Cd). Metallic Cd catalytic reduction of NO_3^- to NO_2^- is very effective. Since the NO_3^- sample size we intend to produce is $\sim 100\text{nmol}$ in 12.8mmol of NO_2^- , the NO_2^- salt used must be 99.9999% pure in order to obtain accurate isotope data from O_3 reacted NO_3^- . Cd is ideal as it will reduce NO_3^- without the need for additional chemical reactants to be added to the solution.

Cd offers great NO_3^- reduction efficiency in various forms. Granular Cd allows for the simplest reduction as it only requires the Cd granule's surface to be cleaned and placed in solution for reduction of NO_3^- to occur. However, granular Cd doesn't have high enough reduction efficiency with 85% of NO_3^- is reduced to NO_2^- (V.V.Nikonorov et al., 2000). "Spongy" Cd is an activated form of Cd with greater reduction efficiencies (96.4%) but this was also insufficient (Deng et al., 2001). Copperized Cadmium (CuCd), another form of activated Cd that used a thicker copper coating, seemed to be the only potential option as it was reported to have 100% reduction efficiency. However this could be misleading as even 99.9999% reduction would be insufficient and thus CuCd must be tested before it is assumed to be applicable for our solutions. CuCd is expected to facilitate reduction of NO_3^- to NO_2^- by the Cu coating acting as a cathode, allowing for more efficient electron flow between Cd and NO_3^- (Jia-Zhong Zhang et al., 2000).

CuCd production proved to be problematic. Methods to produce CuCd granules were simple but often required longer reaction times and produced a poor copper coating (Martha N.Jones, 1984). The common element between all methods was the use of copper sulfate (CuSO_4) in solution which Cd granules are then added and agitated to

allow for the coating to form. This produced a great deal of “Colloidal Copper”, fine Cd fragments, and CuSO_4 solution waste. Colloidal copper was a fine grain cluster of expelled copper that must be removed from the agitation vessel in order for Cd copper coating to continue. Since Cd is a soft metal, the constant agitation caused the granules to erode each other and produce fine Cd fragments, which also reduced the total amount of CuCd produced. Finally, CuSO_4 was in excess in solution to drive the coating reaction and there was significant excess remaining once granule production was completed which could not be reused. All of these waste products accumulated in great volume and had to be stored and processed which was exceptionally time consuming so a more modern approach was needed.

The “Rapid Assay” method proved to be most effective method for producing CuCd (Cortas et al., 1990; Kranti Sorte et al., 2010). This method was a modification of an earlier method that now used a greater CuSO_4 concentration (0.2M) in a glycine buffer solution (0.2M adjusted to 9.7pH) to have a thicker Cu coating applied in a shorter time (~30s). Figure 3 shows the expected CuCd granule appearance after the coating reaction and clearly the “Rapid Assay” method produced the most effective coating. The method also was beneficial due to its limited waste production as it made no colloidal copper, Cd fragments, and small volumes of excess CuSO_4 solution.



Figure 3.3: CuCd granules produced from both methods (Cortas et al., 1990)

CuCd batch and column reduction were compared using the prepared granules. The batch reduction method entailed CuCd granules being placed in a bottle with a NO_3^- test solution and being agitated on a shaker table (120rpm) for 1-30min. The column reduction method involved a glass column packed with CuCd granules and the NO_3^- test solution was allowed to slowly flow through the column. In both instances the test solution was collected after reduction and analyzed via HPLC to see if any observable NO_3^- remained. As expected, both methods converted nearly all of the NO_3^- into NO_2^- and initial tests did not show any NO_3^- in the chromatograph but this was due to the size of the adjacent NO_2^- peak overlapping any potential signal. Later tests used much lower NO_3^- concentrations and peak separation was adequate and residual NO_3^- was present after reduction using both methods (>100ppb). So while reduction in most studies reduction of NO_3^- to NO_2^- can be considered to be 100%, it does not actually go to

completion and is therefore insufficient to allow for the minimal sample size of 100nmol NO_3^- to be isotopically analyzed.

3.6 Removing Residual NO_2^- From Bubbling Solution

O_3 reacting with NO_2^- only creates a small amount of NO_3^- and the excess NO_2^- must be removed prior to isotopic analysis of the NO_3^- . The NO_2^- solution concentration (64mM) for reaction with O_3 was chosen because of its high scrubbing efficiency (99%) which could allow for collection times of ~30min assuming 50ppbv O_3 concentrations. The 200mL of solution used in each trial has 12.8mmol of NO_2^- which is in great excess and must be removed before isotopic analysis of the analyte NO_3^- can be performed. Only 100nmol of NO_3^- is required to get $\delta^{18}\text{O}$ which is ideal since the lower the amount of NO_3^- needed the greater the time resolution of sampling. The small sample size can also be problematic since NO_2^- can interfere with isotopic analysis. NO_2^- undergoes the same reaction in the bacterial denitrification method(section 3.7.2) as NO_3^- to produce N_2O gas which then dilutes or even completely washes out any NO_3^- signal related to O_3 enrichment.

NO_2^- removal presents new challenges such as potential isotopic exchange. Using azidoic or sulfamic acid to remove residual NO_2^- can potentially catalyze oxygen exchange as nitrous acid will exchange with water and then readily exchanges with nitric acid causing a two-step water/ NO_3^- oxygen exchange(C.A.Bunton et al., 1953). This is important because the oxygen isotopic signal ($\Delta^{17}\text{O}$, $\delta^{17}\text{O}$, $\delta^{18}\text{O}$) would be representative of water and not O_3 . If NO_3^- were the only anion present in solution, oxygen exchange would not be an issue since pH must be <1 in order for significant exchange to

occur (C.A. Bunton et al., 1952). NO_2^- more readily undergoes oxygen exchange with water under acidic conditions and catalyzes oxygen exchange between NO_3^- and water (C.A. Bunton et al., 1953); (Bunton et al., 1959). The exchange was examined by adding various amounts of a known NO_3^- standard to a stock NO_2^- solution and removing the excess NO_2^- by the azide reaction method (section 3.6.1). The internal NO_3^- standard known as “Hoffman” has a known $\Delta^{17}\text{O} = 21\text{‰}$ and would be the expected value after NO_2^- removal since it would be the only source of mass independent signal. NO_3^- was isotopically analyzed using the thermal decomposition method (section 3.7.1) as was “Hoffman” NO_3^- control samples that were converted to AgNO_3 directly. The remaining NO_2^- and NO_3^- blank could be calculated by how much the $\Delta^{17}\text{O}$ signal deviates from the known standard in a mass balance. If all samples showed identical amounts of blank then isotopic exchange either doesn't occur or is identical across the examined NO_3^- concentrations. The varied values of $\Delta^{17}\text{O}$ (Fig 3.4) are expected as a consistent blank would dilute $\Delta^{17}\text{O}$ signal proportionally to the amount of NO_3^- added. Oxygen exchange is clearly occurring since as NO_3^- in solution increases, so does blank quantity (Fig 3.5). NO_2^- solutions were made and processed identically, so it is not the blank that is actually increasing. Instead, oxygen exchange between NO_3^- and water is producing more NO_3^- with $\Delta^{17}\text{O} = 0\text{‰}$ which will then be calculated as blank. Had future tropospheric O_3 sampling tests been successful, a calibration between expected NO_3^- concentration and oxygen isotopic exchange would be needed to arrive at an accurate $\Delta^{17}\text{O}$ value of the reacted O_3 .

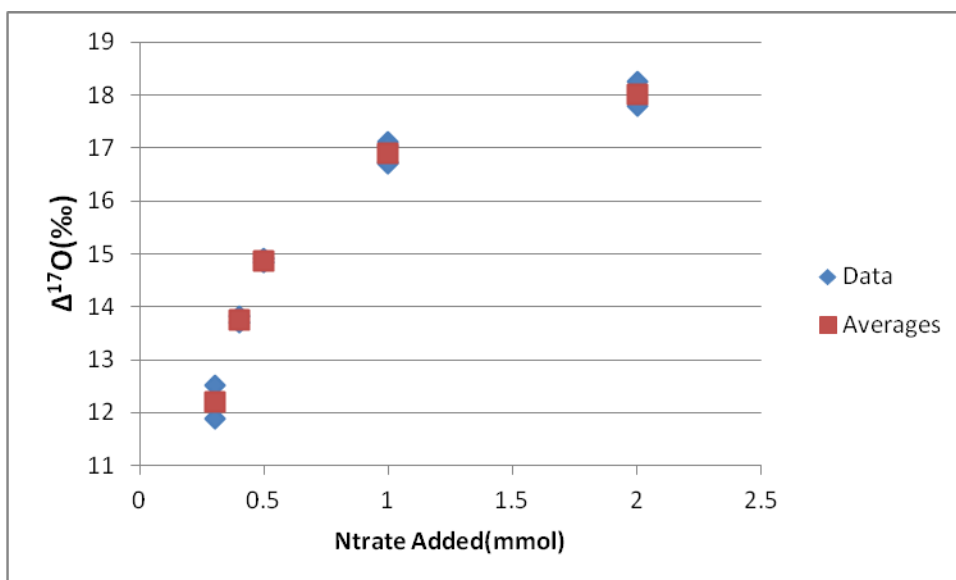


Figure 3.4: $\Delta^{17}\text{O}$ measured from Hoffman NO_3^- isolated from a NO_2^- solution.

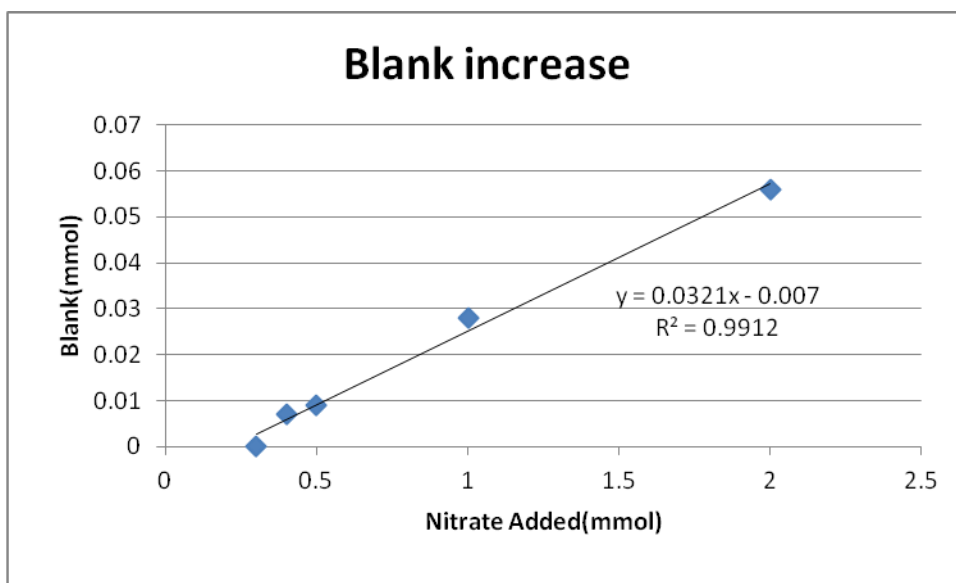


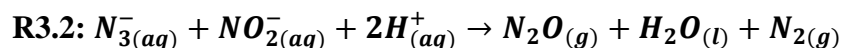
Figure 3.5: Blank increase when baseline blank is considered the amount present in the solution with the smallest NO_3^- added.

NO_2^- removal efficiency was tested via ion chromatography(IC). Ideally NO_2^- removal would be 100% efficient but since this is unlikely, removal to level below the low detection limit(100ppb) could be corrected for in the final data. Typical ion

chromatographs for a for an NO_2^- removal test solution had incomplete NO_2^- removal and while a combination of azide reaction and sulfamic acid addition can reduce NO_2^- levels to below detection limits it is unlikely that this can be done without significant oxygen exchange occurring given the amount of NO_2^- present.

3.6.1 NO_2^- Removal by Reaction with Azide

Reaction with azide is an effective means to eliminate excess NO_2^- . The reaction(R3.2) is ideal because the unwanted NO_3^- is removed from the solution entirely and not transformed into another unwanted molecule. Azide reacts with NO_2^- under acidic conditions to form gas phase nitrous oxide and diatomic nitrogen which bubble out of solution and are evacuated in a fume hood. Reactions were done in a Erlenmeyer flask with a spin bar to agitate the solution and were relatively quick as 12.8mmol of NO_2^- could be removed from solution in ~15min. Reaction rate was acidity dependent since acid was the only component that could be added in excess to drive the reaction.



This was done with the addition of cation exchange resin because adding acid directly like sulfuric or hydrochloric would only result in NO_2^- and azide being replaced by chloride or sulfate. Using H^+ form of cation exchange resin was an ideal source of acidity since the sodium and potassium cations in solution would preferentially bind to the resin releasing protons and thereby driving the reaction. This also served to remove excess cations from solution as well while unwanted NO_2^- reacted and degassed. Once completed ~99% of NO_2^- was removed which is insufficient since NO_3^- sample size is

~100nmol and 1% residual NO_2^- is 128,000nmol. Therefore further processing was necessary but the azide reaction provided a quick reaction to remove the bulk of the NO_2^- .

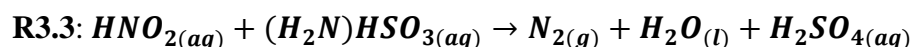
Control solution analysis was difficult due to poor IC peak separation between NO_3^- and azide. Just as with residual NO_2^- analysis, residual azide had to be assessed due to its potentially harmful effects on later isotopic analysis. Since the NO_2^- removal reaction was under titrated with azide there should be none remaining in solution but control tests were required to determine how long complete removal would take. Test solutions were made with NO_2^- only as any addition of NO_3^- would make azide concentration determination exceptionally difficult. This is because NO_3^- and azide have nearly identical retention times when performing anion concentration analysis using HPLC. Despite testing solutions with no added NO_3^- , azide determination was limited as NO_2^- solutions contain significant blank NO_3^- and the amount of azide being detected was <1ppm. Qualitative assessment azide/ NO_3^- peak size seemed to indicate that nearly all azide was removed after 15 min but further testing using the bacterial denitrifier method would ultimately determine if harmful levels remained.

While the azide reaction is very effective of removing NO_2^- , it has several drawbacks. The main issue is that the azide/ NO_2^- removal reaction (R3.2) requires significant acidity which causes oxygen exchange that dilutes the $\Delta^{17}\text{O}$ signature we are interested in. Also, none of the discussed NO_2^- solution processing reactions provide any isotopic data and therefore must be coupled with other methods to arrive at the oxygen enrichment measurements we are interested in. Most NO_3^- isotopic analysis was done using thermal decomposition of AgNO_3 which is problematic when azide is used to react with NO_2^- at residual azide with form AgN_3 which is a contact explosive that could damage lab

equipment and harm lab staff. The bacterial denitrifier method was also used to obtain oxygen isotopic data from NO_3^- but again if residual azide is present this method is not functional as bacteria are killed with minimal azide concentration and therefore unable to convert NO_3^- into nitrous oxide gas (Fisher Scientific, 1999).

3.6.2 NO_2^- Removal with Sulfamic Acid

Reaction with sulfamic acid was used to eliminate residual NO_2^- that was not removed using azide and still allow for isotopic analysis via bacterial denitrification. Addition of sulfamic acid will reduce sample solution to a $\text{pH} < 2$ but in comparison to the acidity and hazards associated with azide it is a vast improvement. The azide reaction is still ideal since all unwanted molecules are completely removed from solution by conversion to gas phase products but remaining NO_2^- must still be removed and that is where sulfamic acid becomes ideal.



The reaction between sulfamic acid and NO_2^- (R3.3) produces water and sulfuric acid that remain in solution and N_2 gas that degasses. The amount of NO_2^- that can be removed has been reported to be up to 7 times the amount of NO_3^- present in solution but others have shown that it can be used to remove significantly larger quantities (Julie Granger et al., 2009; Krystin Riha, 2013). The greatest benefit of sulfamic acid NO_2^- removal is that it allows for data collections using bacterial denitrification. The sulfuric acid produced in the reaction can be neutralized with a base and the salinity of the solution is still sufficiently low to not affect N_2O production or cause significant oxygen exchange. Previous work examined much greater concentrations (500 μmol) of residual NO_2^- and

showed reaction times of ~3min but with such a small NO_3^- sample size (~100nmol) the reaction must be run much longer(hours) to achieve sufficient NO_2^- removal(Julie Granger et al., 2009).

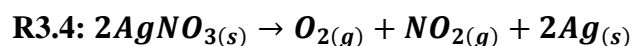
3.7 NO_3^- Processing Methods

NO_3^- must be processed or transformed into a useable form before direct detection of oxygen isotope variation. When O_3 reacts with NO_2^- in solution it forms aqueous NO_3^- . When using the Delta V IRMS in its current configuration, isotopic analysis requires that samples be in the gas phase and are between 18m/z and 46m/z. If NO_3^- were to be introduced in the gas phase it would still exceed m/z limitations as singly charged NO_3^- would be 62 m/z. Therefore, NO_3^- in solution must undergo so reaction before $\delta^{17}\text{O}$, $\delta^{18}\text{O}$, $\Delta^{17}\text{O}$ can be obtained. Our chosen methods are thermal decomposition of AgNO_3 , which produces $\text{O}_{2(g)}$, and bacterial denitrification, producing N_2O or O_2 .

3.7.1 Silver NO_3^- Thermal Decomposition

Silver NO_3^- (AgNO_3) thermal decomposition allows for high precision oxygen isotope analysis of NO_3^- . When heated above 450K AgNO_3 decomposes to produce O_2 (R3.4) gas which is ideal for dual inlet IRMS analysis. The O_2 gas is collected in a sample bellow and directly compared with an O_2 reference gas. Measurements of m/z 32, 33, and 34 correspond to $^{16}\text{O}^{16}\text{O}$, $^{16}\text{O}^{17}\text{O}$, and $^{16}\text{O}^{18}\text{O}$ respectively and allows for the calculation of $\delta^{17}\text{O}$, $\delta^{18}\text{O}$, $\Delta^{17}\text{O}$. Since O_3 supplies 1 oxygen in the formation of NO_3^- to NO_2^- , bulk O_3 $\Delta^{17}\text{O}$ can be approximated as 3 times the $\Delta^{17}\text{O}$ measured from O_2 produce from AgNO_3 decomposition. Multiple replicates of each measurement can be taken in a short

time allowing for high precision data collection as the dual inlet changeover block alternates between sample and reference O₂.



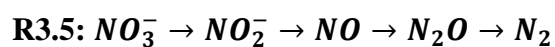
AgNO₃ is produced by a series of reactions and thermally decomposed. NO₃⁻ extracted from the NO₂⁻ bubbler solution would form a NaNO₃ or KNO₃ salt if left in its original form. After acidic azide reaction removes nearly all residual NO₂⁻ and replaces most cations with H⁺, the solution is neutralized by addition and agitation with excess Ag₂O which generates aqueous AgNO₃. The solution is then filtered and frozen before water is removed by sublimation in a freeze dryer. Sublimation allows the water to be removed while leaving a pure AgNO₃ salt which can be measured (~3mg) and placed into a silver capsule for thermal decomposition. While AgNO₃ undergoes thermal decomposition at ~450K, higher temperatures (~500K) will produce a more O₂ consistently and in a shorter time. NO₂ is also produced from the thermal decomposition reaction which must be removed to obtain accurate isotopic measurements from O₂. Both gases are passed through a cryo trap(77K) that is cooled with liquid nitrogen and NO₂ readily condenses while O₂ vapor pressure is sufficiently low to allow it to pass. O₂ is then trapped on a sieve in a collection tube under liquid nitrogen. The collected O₂ can then be allowed to expand into the dual inlet bellow system of IRMS analysis. All of these collection and reaction processes are very labor intensive and difficult to automate as decomposition and collection are very condition sensitive and gas transfer lines must be cleared under vacuum pressure between O₂ collections. Finally, while AgNO₃ thermal decomposition provides the more precise data collection it is sample size limited (at least

2mg, 12 μ mol AgNO₃) because of the required O₂ pressure in the sample bellow to perform the necessary replicate measurements.

3.7.2 Bacterial Denitrification

Denitrification is the ideal method for oxygen isotopic analysis of NO₃⁻ solutions. Any experiment examining a natural system will have a large volume of samples since the non-pristine nature of the sampling will require a high number of replicates to produce reasonable precision. This mean that a large number of NO₃⁻ solutions will need to be processed in order to examine tropospheric O₃ had the bubbling apparatus and NO₂⁻ removal functioned well enough with such low concentrations. The bacterial denitrifier method is therefore ideal since once NO₃⁻ is introduced to a bacterial solution in a closed vial, the rest of the isotopic analysis can be automated which dramatically improves throughput over manual methods. Also, AgNO₃ thermal decomposition required at least 12 μ mol of NO₃⁻ whereas denitrification requires ~100nmol for $\delta^{18}\text{O}$ and ~500nmol for $\delta^{17}\text{O}$, and $\Delta^{17}\text{O}$.

Bacterial denitrification utilizes *Pseudomonas aureofaciens* to produce a N₂O gas from NO₃⁻ which can be used for isotopic analysis of the NO₃⁻. A dilute NO₃⁻ solution is introduced into a bacterial solution and *pseudomonas aureofaciens* are a species that will sequentially reduce NO₃⁻ (R3.5) known as denitrification (Casciotti et al., 2002;Reddy et al., 1984). Most denitrifying bacteria will reduce NO₃ all the way to N₂ but *Pseudomonas aureofaciens* provides incomplete denitrification stopping at N₂O.

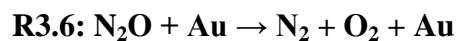


N_2O then degasses from the bacterial solution and is trapped in the headspace of the reaction vial where it remains until extraction. An autosampler is used to extract gas from the vial headspace with a helium back pressure and the N_2O is passed through a series of chemical traps removing unwanted components such as water vapor and carbon dioxide and is then condensed in a series of cryo traps which focuses the N_2O gas to allow for greater signal intensity. N_2O analysis can only provide $\delta^{18}\text{O}$ values because while 46 m/z is almost exclusively from presence of ^{18}O not 2 ^{15}N atoms, the presence of a single ^{15}N is more likely than 45 m/z from ^{17}O . Therefore N_2O can provide information on ^{15}N enrichment, further gas reactions must be performed to obtain $\delta^{17}\text{O}$.

Extensive calibration and data correction is required to insure the accuracy N_2O measured oxygen enrichments. As previously discussed, the presence of residual NO_2^- in solution can dilute the isotopic signature of NO_3^- and this is also true when using bacterial denitrification. *Pseudomonas aureofaciens* process NO_3^- and NO_2^- in the same manner (R3.5) and will reduce NO_2^- to N_2O which will be mixed with N_2O from NO_3^- reduction. This is accounted for in pre-IRMS NO_3^- solution processing but lower than expected enrichment data can suggest that NO_2^- removal was incomplete. Corrections must also be made to account for N_2O dilution from helium carrier gas in the “open split” gas interface. After exiting all the focusing and trapping elements, N_2O enters the IRMS through a capillary that extracts N_2O from the open split, a sample introduction apparatus that allows for continuous gas introduction in an open capillary tube. The large excess of helium mixed with N_2O causes significant deviation from the true isotopic values (Riha et al., 2013). There is also error associated with instrument drift which can be from a number of causes such as ion beam focusing, saturation of contaminant traps, and GC

column retention time drift. To correct for many of these issues, intermittent calibration standards are placed in the sample run so drift can be assessed by how far those standards deviate from their known values. While the automation allows for high sample throughput, post processing data correction can cause error if not handled carefully.

Addition of catalytic gold reduction allows for collection of $\Delta^{17}\text{O}$ data to be acquired. Our primary interest is $\Delta^{17}\text{O}$ signal from NO_3^- so our needs are not met by N_2O analysis alone because of its inability to measure $\delta^{17}\text{O}$. Therefore, N_2O was passed over gold wire heated to 1173K which reduces N_2O to N_2 and O_2 (R3.6)(Kaiser et al., 2006). Product gasses are then separated on a GC column and intensities for $^{16}\text{O}^{16}\text{O}$, $^{16}\text{O}^{17}\text{O}$, and $^{16}\text{O}^{18}\text{O}$ are measured allowing for the calculation of $\delta^{17}\text{O}$, $\delta^{18}\text{O}$, and $\Delta^{17}\text{O}$. A downside to this method is that the $\sim 100\text{nmol}$ required for N_2O analysis is insufficient and at least $\sim 500\text{nmol}$ must be added to the bacteria for enough O_2 gas to be produced for reliable measurements of $\Delta^{17}\text{O}$.



3.8 Potential Improvements

Effective tropospheric O_3 collection is limited by the required minimum sample size for isotopic analysis. Assuming 10ppb_v O_3 concentration, 500nmol of NO_3^- could be produced from reaction with NO_2^- in the bubbler in $\sim 12\text{hrs}$ which is reasonably fine temporal resolution. However with the limitations of the NO_2^- removal processes and amount of NO_3^- blank in solution, 1mmol of NO_3^- would likely be needed to obtain accurate isotopic data and bubbler collection time would have to be extended to $\sim 10\text{days}$. But assuming an improved solution processing method were developed, sample size

limitations would be dependent upon the dilution associated with the open split gas introduction interface. If this were bypassed and the gas inlet capillary could be directly connected to the ion source, the lack of dilution would intensify the signal intensity and allow for smaller amounts of NO_3^- to be needed and would improve temporal resolution.

Significantly altering the atmospheric gas sampling apparatus could allow for greater sample collection. The bubbling apparatus described in section 3.3 allows for 99% O_3 scrubbing efficiency and while this may seem near perfect, the large amounts of NO_2^- needed in the bubbling solution make it not ideal. Maintaining high scrubbing efficiencies while decreasing the amount of NO_2^- needed could be possible based on improving the surface area and interaction time between gas phase O_3 and NO_2^- solution. If a finer fritted disk could be used to decrease bubble size, this would increase surface area of each bubble allowing for greater interaction between gas and liquid. A longer column length for the bubbles to travel up would increase reaction time and allow for higher O_3 scrubbing. So while NO_2^- concentration in the 200mL bubbler used in this work needed to be 64mM, finer bubble size and a longer path length would allow a similar volume of solution with lower NO_2^- concentrations to achieve the same effect.

NO_2^- removal reactions and salt purity are the limiting factors in this O_3 sampling method. The small amounts of NO_3^- needed for isotopic analysis is a great asset from a time resolution view but become very limiting because of the high purity NO_2^- solutions required to obtain pure salts capable of producing accurate isotopic measurements. NO_2^- salts of high purity are difficult to maintain as they are hygroscopic and photo sensitive and tend to form NO_3^- blank when left exposed. High purity (>99.999%) NaNO_2 can be purchased but are expensive and have the same limitations as the more functional and

cheaper 99% pure KNO_2 salts. Finding a way to limit formation of any blank NO_3^- in NO_2^- solution with the exception of reaction with O_3 would be ideal but exceptionally difficult. However, it would be much more plausible through extensive control tests to determine if NO_3^- blank concentration could be simplistically related to bubbler conditions which would allow for calibration of final data. Calibration would still be very difficult because NO_2^- removal reactions have been shown to cause oxygen isotopic exchange with water and a non-acidic NO_2^- removal reaction or high concentration separation technique is needed to eliminate this problem.

3.9 Conclusions and Implications

Tropospheric O_3 remains difficult to sample from bulk atmospheric gas due to its low concentration. With current NO_3^- blank concentrations in NO_2^- solutions a large amount of O_3 (1mmol) would have to be reacted to produce enough sample NO_3^- to result in accurate isotopic measurements. In most locations this would take up to 10 days and would still be unreliable as high gas flow through NO_2^- solution causes significant evaporation which limits scrubbing efficiency. The method in its current form cannot be used for low concentration O_3 analysis except potentially in high pollution locations such as dense cities or industrial complexes as their high VOC and NO_x emissions can cause concentrations to exceed 75ppb_v which would reduce sampling time to ~32hrs(EPA, 2012b).

If NO_2^- solution sampling can be done, it offers unique information about terminal O_3 enrichment. Reaction with NO_2^- was specifically chosen because O_3 's terminal oxygen is almost exclusively the reactive atom and is considered the source of most of

the $\Delta^{17}\text{O}$ signature found in atmospheric molecules. O_3 formation's mass independent enrichment is unique and while bulk O_3 has been collected and isotopically analyzed, enrichment of the terminal atom alone has not been achieved (Johnston et al., 1997). Chapter 2 attempts to derive terminal enrichment from measured $\delta^{17}\text{O}$ and $\delta^{18}\text{O}$ of bulk O_3 through experimental relationships but direct sampling would potentially provide observations to validate or refute those calculations.

Terminal O_3 enrichment can be used in a variety of atmospheric reaction studies. Because mass independent fractionation is so uncommon, reaction with O_3 can be assumed when high $\Delta^{17}\text{O}$ is observed. This provides a useful method to study atmospheric reaction mechanisms and specifically cleansing mechanisms as only species with some direct or indirect O_3 reaction will have a significant $\Delta^{17}\text{O}$. Since O_3 is highly reactive this means reactions with NO_x , SO_x , and HO_x , can be better understood if terminal enrichment of O_3 is defined. Current O_3 enrichment data provides much evidence as to its reaction pathways but quantitation reaction kinetics and pathway preference will be limited until direct observation of terminal $\Delta^{17}\text{O}$ can be associated with atmospheric conditions.

CHAPTER 4. CONCLUSIONS

Laboratory findings can be used to determine $\delta^{18}\text{O}$ and $\Delta^{17}\text{O}$ values of O_3 formed at tropospheric temperatures and pressure. The open flow photolysis chamber experiment yielded temperature dependent slopes for $\delta^{17}\text{O}$, $\delta^{18}\text{O}$, and $\Delta^{17}\text{O}$ of 0.2385, 0.3216, 0.0649 respectively. In the experimental temperature range (273K-320K), $\delta^{17}\text{O}$ was found to be between 70.9-81.6‰ with $\delta^{18}\text{O}$ between 72.4-87.0‰. Previous works yielded much less precise isotopic enrichment data which therefore did not allow for a conclusion to be drawn about whether temperature and pressure effects were independent from each other. As they are often considered to be independent of each other and our $\delta^{17}\text{O}$ data was in agreement with this assertion, temperature and pressure independence was assumed for future photochemical box model predictions.

O_3 's isotopic enrichment is expected to vary between the central and terminal atom, so asymmetric and symmetric must be predicted independently. Symmetric O_3 is expected have $\Delta^{17}\text{O} = 0\text{‰}$, which means measured $\Delta^{17}\text{O}$ from bulk O_3 resides in the asymmetric species. The ratio of isotopic enrichment (r50) between the two isotopomers also doesn't follow the statistical prediction of 2 to 1. By assuming only that symmetric O_3 $\Delta^{17}\text{O} = 0\text{‰}$ and that r50 can be predicted from measured bulk O_3 enrichment, $\Delta^{17}\text{O}^a$ was predicted to be between 45.2‰ and 50.9‰. These values can be impactful in

prediction of $\Delta^{17}\text{O}$ in other atmospheric molecules such as NO_x and SO_x as they are isotopically enriched through O_3 terminal atom extraction.

Determining the isotopic composition of tropospheric O_3 using nitrite was unsuccessful but can still provide information about terminal isotopic enrichment when reacting with higher O_3 concentrations. Nitrate blank in bubbling solutions limited the minimum sample size as any non- O_3 reacted nitrate in solution will dilute the isotopic enrichment signal. Nitrate blank will have $\Delta^{17}\text{O} = 0\%$ which will need to be corrected for using a mass balance but should not exceed 10% of total sample nitrate quantity. Isotopic enrichment signal dilution can also come from acidic oxygen exchange between water and nitrate. Exchange is catalyzed by the presence of nitrite, which is in great excess in our bubbling solutions. Exchange was directly measured through control experiments and can be corrected for as long as nitrate concentration in solution is known before nitrite removal reactions are performed. Once isolated, nitrate can be used to calculate the terminal $\Delta^{17}\text{O}$ of O_3 as 1 of the 3 oxygen atoms is from reaction with O_3 while the other two will have $\Delta^{17}\text{O} = 0\%$. Therefore measured $\Delta^{17}\text{O}$ of nitrate can be multiplied by 3 to arrive at $\Delta^{17}\text{O}^a$ of bubbled O_3 .

4.1 Future Work

Isotopic enrichment of O_3 formed by photolysis and electric discharge in an open flow system should be investigated. Previous work has used a closed reaction system in which O_3 is formed over long photolysis or discharge times and usually collected on the vessel wall. However, this reaction apparatus could lead to extensive oxygen exchange between O , O_2 , and O_3 , which could alter the terminal isotopic signature of measured

product O_3 . The open flow system used for Chapter Two experiments would be ideal as the short photolysis times would limit the time for the exchange processes to occur and allow for post O_3 formation reactions to be performed to measure terminal isotopic enrichment.

Isotopic enrichment of laboratory O_3 must also be studied as a function reaction time to determine if exchange processes are mixing enrichment from the terminal to the central atom. With the proposed experimental setup we could vary photolysis or discharge times by either covering different lengths of the photolysis chamber to block the light source or by changing the depth of the salt solution. This would answer the question of whether reaction time has a significant effect on bulk O_3 isotopic enrichment. When coupled with nitrite bubbling solution (Chapter 3), O_3 's terminal atom could be reacted and its isotopic enrichment measured to be compared to bulk O_3 . Isotopic measurements are very sensitive to exchange processes and if reaction time does cause a significant effect it may also demonstrate a measureable exchange between O_3 , O_2 , and O . This could potentially relate the magnitude of terminal enrichment to reaction time or even demonstrate the potential for mass independent isotopic enrichments to be present in the symmetric form of O_3 .

Additional experiments that determine central versus terminal enrichment in O_3 should be conducted. Chapter 2 data only examines isotopic enrichment as a function of temperature for bulk O_3 . With simultaneous collection of gas phase O_3 and terminal oxygen reaction with nitrite the isotopic enrichment of asymmetric and symmetric O_3 can be measured directly. This would allow for the assumptions of the photochemical box model (Chapter 2) to be replaced with observed data. Terminal oxygen isotopic

enrichment measured from collected nitrate also allows for comparison of r_{50} dependence on temperature and pressure with previous studies. This could validate the predictions of Model 3 or provide insight into possible corrections to that model.

4.2 Implications

Understanding the effects of temperature, pressure, and reaction time on isotopic enrichment associated with O_3 formation could show agreement between studies that report different values. The many laboratory studies of O_3 isotopic enrichment often vary by over 10‰ and lead to different conclusions to be drawn about the source of O_3 's unique isotopic signature. The data presented in this thesis as well as the potential future work could shed light on the reason for differences in isotopic enrichment magnitude between experiments. An open flow system was used to provide conditions similar to an open atmosphere and the proposed reaction duration dependent study would allow for the determination of possible isotope effects that are not a function of temperature or pressure. If these effects are present it should be examined further to determine if isotopic exchange processes affect O_3 's $\Delta^{17}O$ signature significantly.

Abstraction of O_3 's terminal atom with reaction with nitrite could improve our understanding of mass independent fractionation. Direct measurement of O_3 's terminal isotopic enrichment has been done by reaction with silver, but nitrite reaction data is sparse. The nitrite bubbling reaction offers a high efficiency way to make these direct measurements that are otherwise very difficult to obtain from other methods such as laser spectroscopy. All mass independent isotopic enrichment is expected to reside in the asymmetric form of O_3 but without reliable measurements this assumption cannot be

validated. If exchange processes do occur that transfer the mass independent signature to symmetric O₃, then the duration of the formation/destruction reaction should yield different terminal isotopic enrichment values. This would then change the predicted mass independent enrichment of various atmospheric species that result from abstraction a terminal O atom from reaction with O₃.

Once terminal enrichment of O₃ is better defined, enrichment of other species in the atmosphere can be modeled and predict how $\Delta^{17}\text{O}$ is transferred. If mass independent enrichment can be directly related to temperature, pressure, and UV exposure during formation, then subsequent atmospheric reactions with O₃ can be better understood. Mass independent enrichment provides a useful tracer that can be used to understand reaction mechanisms and kinetics as long as the initial isotopic enrichment magnitude is known. Atmospheric molecules that have a positive $\Delta^{17}\text{O}$ signature could then be used to examine atmospheric transport or even secondary reactions that transfer an O atom to another molecule.

LIST OF REFERENCES

LIST OF REFERENCES

- Bhattacharya, S. K., A. Pandey and J. Savarino, Determination of intramolecular isotope distribution of ozone by oxidation reaction with silver metal, *Journal of Geophysical Research-Atmospheres*, 113, 2008.
- Brown, J. H., K. M. Cook, F. G. Ney and T. Hatch, Influence of Particle Size upon the Retention of Particulate Matter in the Human Lung, *American Journal of Public Health and the Nations Health*, 40(4), 450-480, 1950.
- Bunton, C. A., E. A. Halevi and D. R. Llewellyn, Oxygen Exchange Between Nitric Acid and Water. Part 1, *J. Chem. Soc.*, 4913-4916, 1952.
- Bunton, C. A., D. R. Llewellyn and G. Stedman, Oxygen Exchange between Nitrous Acid and Water, *J. Chem. Soc.*, 568-573, 1959.
- C.A.Bunton and E.A.Halevi, Oxygen exchange between nitric acid and water. Part II, *Journal of the Chemical Society*, 4917-4924, 1952.
- C.A.Bunton, E.A.Halevi and D.R.Llewellyn, Oxygen exchange between nitric acid and water. Part III. Catalysis by nitrous acid., *Journal of the Chemical Society*, 2653-2657, 1953.
- C.David, A.Haefele, P.Keckhut, M.Marchand, J.Jumelet, T.Leb Blanc, C.Cenac, C.Laqui, J.Porteneuve, M.Haefelin, Y.Courcoux, M.Snels, M.Viterbini and M.Quatrevalet, Evaluation of stratospheric ozone, temperature, and aerosol profiles from the LOANA lidar in Antarctica, *Polar Science*, 6, 209-225, 2012.
- C.Janssen, Intramolecular isotope distribution in heavy ozone, *Journal of Geophysical Research*,(110), 2005.
- Casciotti, K. L., D. M. Sigman, M. G. Hastings, J. K. Böhlke and A. Hilkert, Measurement of the oxygen isotopic composition of nitrate in seawater and freshwater using the denitrifier method, *Anal. Chem.*, 74(19), 4905-4912, 2002.
- Cortas, N. and Wakid NW, Determination of Inorganic Nitrate in Serum and Urine by a Kinetic Cadmium-Reduction Method, *Clinical Chemistry*, 36(8), 1440-1443, 1990.

- Costa, A., G. Michalski, A. Schauer, B. Alexander, E. Steig, E. Sofen and P. Shepson, Analysis of atmospheric inputs of nitrate to a temperate forest ecosystem from Delta O-17 isotope ratio measurements, *Geophysical Research Letters*, 38, 2011.
- Criss, R. E., Principles of stable isotope distribution /, Oxford University Press, New York, 1999.
- Deng, J., C. Lu, J. Zhang and Y. Yuan, Determination of Nitric Oxide in Serum by Activated Spongy Cadmium on Microscale Chromatographic Column, *Progress in Biochemistry and Biophysics*, 28(4), 579-581, 2001.
- Dutsch, H. U., The Ozone Distribution in the Atmosphere, *Canadian Journal of Chemistry*, 52, 1973.
- Edmond de Hoffman and Vincent Stroobant, Mass Spectrometry: Principles and Applications, Wiley-Interscience, 2007.
- EPA, National ambient air quality standards(NAAQS), 2012a.
- EPA, What is Ozone?, 2012b.
- EPA, Health Effects of Ozone in the General Population, 2013.
- F.Sherwood Rowland, Stratospheric ozone depletion, *Philosophical Transactions of the Royal Society*, 361(1469), 769-790, 2006.
- Fisher Scientific, MSDS Sodium Azide, 1999.
- Gabriel Bowen, Waterisotopes.org, 2013.
- Gao, Y. Q. and R. A. Marcus, Strange and unconventional isotope effects in ozone formation, *Science*, 293(5528), 259-263, 2001.
- Gao, Y. Q. and R. A. Marcus, On the theory of the strange and unconventional isotopic effects in ozone formation, *J. Chem. Phys.*, 116(1), 137-154, 2002.
- Hanson, D. and K. Mauersberger, The Vapor-Pressures of Solid and Liquid Ozone, *J. Chem. Phys.*, 85(8), 4669-4672, 1986.
- Heidenreich, J. E., III and M. H. Thiemens, A non-mass-dependent isotope effect in the production of ozone from molecular oxygen, *J. Chem. Phys.*, 78(2), 892-895, 1983.
- Heidenrich, J. E. and M. H. Thiemens, A non-mass-dependent oxygen isotope effect in the production of ozone from molecular oxygen: the role of molecular symmetry in isotope chemistry, *J. Chem. Phys.*, 84(4), 2129-2136, 1986.

- J.L.Pinedo V., F Mireles G., C.Rios M., L.L.Quirino T. and J.I.Davila R., Spectral signature of ultraviolet solar irradiance in Zacatecas, *Geofisica Internacional*, 45(4), 263-269, 2006.
- J.P.Burrows, A.Richter, A.Dehn, B.Deters, S.Himmelmann, S.Voigt and J.Orphal, Atmospheric remote-sensing reference data from GOME-2. temperature dependent absorption cross sections of O₃ in the 231-794nm range, *Journal of Quantum Spectroscopy and Radiative Transfer*, 61(4), 509-517, 1999.
- James C.Ianni, Kintecus, 2002.
- Janssen, C., J. Guenther, D. Krankowsky and K. Mauersberger, Temperature dependence of ozone rate coefficients and isotopologue fractionation in O-16-O-18 oxygen mixtures, *Chem. Phys. Lett.*, 367(1-2), 34-38, 2002.
- Janssen, C., J. Guenther, D. Krankowsky and K. Mauersberger, Temperature dependence of ozone rate coefficients and isotopologue fractionation in O-16-O-18 oxygen mixtures, *Chem. Phys. Lett.*, 367(1-2), 34-38, 2003.
- Janssen, C., J. Guenther, K. Mauersberger and D. Krankowsky, Kinetic origin of the ozone isotope effect: a critical analysis of enrichments and rate coefficients, *Phys. Chem. Chem. Phys.*, 3(21), 4718-4721, 2001.
- Jean-Claude Wolff, Ulf Ornemark, Philip D.P.Taylor and Paul De Bievre, Stability studies and purification procedure for nitrite solutions in view of the preparation of isotopic reference materials, *Talanta*, (46), 1031-1040, 1997.
- Jia-Zhong Zhang, Charles J.Fischer and Peter B.Ortner, Comparison of open tubular cadmium reactor and packed column in automated gas-segmented continuous flow nitrate analysis, *International Journal of Environmental Analytical Chemistry*, 76(2), 2000.
- Johnston, J. C. and M. H. Thiemens, The isotopic composition of tropospheric ozone in three environments, *J. Geophys. Res.*, 102(D21), 25395-25404, 1997.
- Julie Granger and Daniel M.Sigman, Removal of nitrite with sulfamic acid for nitrate N and O isotope analysis with the denitrifier method, *Rapid Communications in Mass Spectrometry*, (23), 3753-3762, 2009.
- Kaiser, J., M. G. Hastings, B. Z. Houlton, T. Rockmann and D. M. Sigman, Triple Oxygen Isotope Analysis of Nitrate Using the Denitrifier Method and Thermal Decomposition of N₂O, *Analytical Chemistry*, 79, 599-607, 2006.
- Kaye, J. A., Theoretical analysis of isotope effects on ozone formation in oxygen photochemistry, *J. Geophys. Res.*, 91(D7), 7865-7874, 1986.

- Kaye, J. A. and D. F. Strobel, Enhancement of heavy ozone in the Earth's atmosphere?, *J. Geophys. Res.*, 88(13), 8447-8452, 1983.
- Krankowsky, D., P. Lammerzahl and K. Mauersberger, Isotopic measurements of stratospheric ozone, *Geophys. Res. Lett.*, 27(17), 2593-2595, 2000.
- Kranti Sorte and Anjan Basak, Development of a modified copper-cadmium reduction method for rapid assay of total nitric oxide, *Analytical Methods*, 2(7), 944-947, 2010.
- Krystin Riha, The Use of Stable Isotopes to Constrain The Nitrogen Cycle, Purdue University, 2013.
- Kunasek, S., B. Alexander, E. Steig, E. Sofen, T. Jackson, M. H. Thiemens, J. McConnell, D. Gleason and H. Amos, Sulfate sources and oxidation chemistry over the past 230 years from sulfur and oxygen isotopes of sulfate in a West Antarctic ice core, *Journal of Geophysical Research-Atmospheres*, 115, 2010.
- Larsen, R. W., N.W.Larsen, F.M.Nicoaisen, G.O.Sorensen and J.A.Beukes, Measurements of ^{18}O -Enriched Ozone Isotopomer Abundances Using High-Resolution Fourier Transform Far-IR Spectroscopy, *Journal of Molecular Spectroscopy*, 200, 235-247, 2000.
- Liu, Q., L. M. Schurter, C. E. Muller, S. Aloisio, j. s. Francisco and D. W. Margerum, Kinetics and mechanisms of aqueous ozone reactions with bromide, sulfite, hydrogen sulfite, iodide, and nitrite ions, *Inorganic Chemistry*, 40(17), 4436-4442, 2001.
- M.F.Miller, I.A.Franchi, A.S.Sexton and C.T.Pillinger, High precision d^{17}O isotope measurements of oxygen from silicates and other oxides: method and applications, *Rapid Communications in Mass Spectrometry*, 13, 1211-1217, 1999.
- Martha N.Jones, Nitrate Reduction by Shaking with Cadmium, *Water Research*, 18(5), 643-646, 1984.
- Matsuhisa, Y., J. R. Goldsmith and R. N. Clayton, Mechanisms of hydrothermal crystallization of quartz at 250 °C and 15 kbar, *Geochim. Cosmochim. Acta*, 42(2), 173-182, 1978.
- Mauersberger K., Krankowsky, Janssen and Schinke, Assessment of the Ozone Isotope Effect, in ADVANCES IN ATOMIC, MOLECULAR, AND OPTICAL PHYSICS, 2005.
- Mauersberger, K., Measurement of Heavy Ozone in the Stratosphere, *Geophys. Res. Lett.*, 8(8), 935-937, 1981.

- Mauersberger, K., B. Erbacher, D. Krankowsky, J. Gunther and R. Nickel, Ozone isotope enrichment: Isotopomer-specific rate coefficients, *Science*, 283(5400), 370-372, 1999.
- Mauersberger, K., D. Hanson and J. Morton, Precision Ozone Calibration System Based on Vapor-Pressures of Ozone, *Review of Scientific Instruments*, 58(6), 1063-1066, 1987.
- Mauersberger, K., P. Lammerzahl and D. Krankowsky, Stratospheric ozone isotope enrichments-revisited, *Geophys. Res. Lett.*, 28(16), 3155-3158, 2001.
- Mauersberger, K., J. Morton, B. Schueler, J. Stehr and S. M. Anderson, Multi-Isotope Study of Ozone - Implications for the Heavy Ozone Anomaly, *Geophys. Res. Lett.*, 20(11), 1031-1034, 1993.
- Mccabe, J. R., M. H. Thiemens and J. Savarino, A record of ozone variability in South Pole Antarctic snow: Role of nitrate oxygen isotopes, *J. Geophys. Res.*, 112(D12), 2007.
- Michalski, G. and S. K. Bhattacharya, The role of symmetry in the mass independent isotope effect in ozone., 2009.
- Michalski, G., T. Meixner, M. Fenn, L. Hernandez, A. Sirulnik, E. Allen and M. Thiemens, Tracing atmospheric nitrate deposition in a complex semiarid ecosystem using $\Delta^{17}\text{O}$, *Envir. Sci. Tech.*, 38(7), 2175-2181, 2004.
- Miller, M. F., Isotopic fractionation and the quantification of ^{17}O anomalies in the oxygen three-isotope system: an appraisal and geochemical significance, *Geochim. Cosmochim. Acta*, 66(11), 1881-1889, 2002.
- Miller, M. F., I. A. Franchi, M. H. Thiemens, T. L. Jackson, A. Brack, G. Kurat and C. T. Pillinger, Mass-independent fractionation of oxygen isotopes during thermal decomposition of carbonates, *Proceedings of the National Academy of Sciences of the United States of America*, 99(17), 10988-10993, 2002.
- Morton, J., J. Barnes, B. Schueler and K. Mauersberger, Laboratory Studies of Heavy Ozone, *J. Geophys. Res.*, 95(D1), 901-907, 1990.
- NIST, Report of Investigation: Reference Materials 8535, 8536, 8537 , Department of Commerce, 2005.
- NIST, O₂ Molecular Constants, 2012.
- Reddy, R. K., W.H.Patrick and F.E.Broadbent, Nitrogen transformations and loss in flooded soils and sediments, *CRC Critical Reviews in Environmental Control*, 13(4), 273-309, 1984.

- Riha, K. M., M.Z.King, L.Crawley and G.Michalski, Standardization of D17O and d15N using the denitrifier method and gold tube thermal decomposition, (*in prep*), 2013.
- Ryoji Tanaka and Eizo Nakamura, Determination of 17O-excess of terrestrial silicate/oxide minerals with respect to VSMOW, *Rapid Communications in Mass Spectrometry*, 27, 285-297, 2013.
- S.K.Bhattacharya, Subrata Chakraborty, Joel Savarino and Mark H.Thiemens, Low-pressure dependency of the isotopic enrichment in ozone: Stratospheric implications, *Journal of Geophysical Research*, 107, 2002.
- S.P.Sander, R.R.Friedl, D.M.Golden, M.J.Kurylo, R.E.Huie, V.L.Orkin, G.K.Moortgat, A.R.Ravishankara, C.E.Kolb, M.J.Molina and B.J.Finlayson-Pitts, Chemical kinetics and photochemical data for use in atmospheric studies, *JPL Publication*, 14, 1-334, 2003.
- Sanford Sillman, Jennifer A.Logan and Steven C.Wofsy, The Sensitivity of Ozone to Nitrogen Oxides and Hydrocarbons in Regional Ozone Episodes, *Journal of Geophysical Research*, 95, 1837-1851, 1990.
- Savarino, J., S. Morin, J. Erbland, F. Grannec, M. Patey, W. Vicars, B. Alexander and E. Achterberg, Isotopic composition of atmospheric nitrate in a tropical marine boundary layer, *Proceedings of the National Academy of Sciences*, 110(44), 17668-17673, 2013.
- Schueler, B., J. Morton and K. Mauersberger, Measurement of Isotopic Abundances in Collected Stratospheric Ozone Samples, *Geophys. Res. Lett.*, 17(9), 1295-1298, 1990.
- Seinfeld, J. H. and S. N. Pandis, Atmospheric chemistry and physics : from air pollution to climate change, New York : Wiley, 1998.
- Sillman, S., The relation between ozone, NOx, and hydrocarbons in urban and polluted rural environments, *Atmos. Environ.*, 33, 1821-1845, 1999.
- Sofen, E., B. Alexander and S. Kunasek, The impact of anthropogenic emissions on atmospheric sulfate production pathways, oxidants, and ice core Delta O-17(SO42-), *Atmospheric Chemistry and Physics*, 11(7), 3565-3578, 2011.
- Suzanne Clancy, DNA damage & repair: mechanisms for maintaining DNA integrity, *Nature Education*, 1(1), 2008.
- Thiemens, M. H., History and applications of mass-independent isotope effects, *Annual Review of Earth and Planetary Sciences*, 34, 217-262, 2006.

- Thiemens, M. H. and T. Jackson, New experimental evidence for the mechanism for production of isotopically heavy ozone, *Geophys. Res. Lett.*, 15(7), 639-642, 1988.
- UVP, Pen-Ray Mercury Lamps, 2014.
- V.V.Nikonorov and T.A.Belyanskaya, Comparative Study of Various Methods of the Heterogeneous Reduction of Nitrate Ions, *Journal of Analytical Chemistry*, 55, 116-120, 2000.
- Van Wyngarden, A. L., K. A. Mar, K. A. Boering, J. J. Lin, Y. T. Lee, S. Y. Lin, H. Guo and G. Lendvay, Nonstatistical behavior of reactive scattering in the O-18+O-32(2) isotope exchange reaction, *J. Am. Chem. Soc.*, 129(10), 2866-2870, 2007.
- Weather Underground, Historical Weather, 2013.
- William C.Vicars, S.K.Bhattacharya, Joseph Erbland and Joel Savarino, Measurement of the 17O-excess(D17O) of tropospheric ozone using a nitrite-coated filter, *Rapid Communications in Mass Spectrometry*, 26, 1219-1231, 2012.
- Wolf, S., M. Bitter, D. Krankowsky and K. Mauersberger, Multi-isotope study of fractionation effects in the ozone formation process, *J. Chem. Phys.*, 113(7), 2684-2686, 2000.
- Y.Matsumi, F.J.Comes, G.Hancock, A.Hofzumahaus, A.J.Hynes, M.Kawasaki and A.R.Ravishankara, Quantum yields for production of O(1D) in the ultraviolet photolysis of ozone: recommendation based on evaluation of laboratory data, *Journal of Geophysical Research*, 107(D3), 4024, 2002.
- Zhaozhong Feng and Kazuhiko Kobayashi, Assessing the impacts of current and future concentrations of surface ozone on crop yield with meta-analysis, *Atmospheric Environment*, (43), 1510-1519, 2009.

APPENDIX

Table A. 1: Stratospheric ozone measurements.

Year	Mean Alt. (km)	Enrichment(‰)				ref.	
		$^{49}\text{O}_3$	\pm	$^{50}\text{O}_3$	\pm		$\Delta^{17}\text{O}$
1988	33.9	112	12	161	9	27.7	[1]
1988	30.5	107	10	143	6	31.4	[1]
1988	27.5	87	10	121	6	23.4	[1]
1989	33.5	92	17	89	12	43.2	[1]
1989	29.0	81	18	81	15	36.9	[1]
1989	30.6	82	8	91	5	33	[1]
1991	37.1	130	40	230	50	13.3	[2]
1991	33.1	110	17	148	13	31.8	[2]
1991	29.8	91	30	96	20	38.9	[2]
1998	22.4	84.8	7.4	87.3	4.6	37.4	[3]
1998	22.3	75.1	5.3	91.1	3.3	26.6	[3]
1998	22.4	80.5	5.3	92.1	3.5	31.1	[3]
1998	21.6	80	4.9	83.9	3	34.6	[3]
1998	28.9	76.5	4.8	84.6	3	31	[3]
1998	25.4	69.7	4.6	74.5	2.8	29.6	[3]
1998	20.9	69.1	5.1	70.8	3.3	30.8	[3]
1999	30.7	83.5	4.8	92.5	3.1	33.7	[3]
1999	30.7	81.7	4.8	92.9	3	31.8	[3]
1999	29.0	79.1	6.2	90.3	3.9	30.7	[3]
1999	25.6	77.7	4.8	78.6	3	35	[3]
1999	31.8	87.1	5.7	105	3.6	31	[3]
1999	31.8	92.4	5.7	107.8	3.5	34.5	[3]
1999	28.5	81.2	5.4	91.4	3.5	32.1	[3]
1999	23.3	68.4	5.3	80.9	3.4	25.3	[3]

References: [1]-(Schueler et al., 1990), [2]-(Mauersberger et al., 1993), [3]-(Krankowsky et al., 2000)

Table A. 2: Tropospheric ozone measurements

Year	Enrichment(‰)				
	⁴⁹ O ₃	±	⁵⁰ O ₃	±	Δ ¹⁷ O
1995	72	2	90.4	1	24
1995	73.5	3	83.9	0.7	28.6
1995	77.3	2	86.5	0.8	30.8
1995	72.6	6	76.6	1	31.3
1995	67.5	4	77.8	0.3	25.9
1995	86.6	5	88.1	2	38.7
1995	71.8	4	86.8	0.6	25.6
1995	68.3	1	81.5	0.6	24.9
1995	65.9	1	78.2	0.6	24.2
1995	66.9	0.7	81.3	0.5	23.7
1995	66.8	0.6	81.8	0.7	23.3
1995	66	1	82.1	0.7	22.4
1995	67	2	81.4	0.7	23.7
1995	68.7	1	82.1	0.4	24.9
1995	61.7	3	74.4	0.8	22.1
1995	56.6	3	72.7	0.5	18.1
1995	59	2	69.9	1	21.8
1995	61.5	3	77.7	0.6	20.3
1995	63.3	1	76.8	0.6	22.5
1995	64.7	0.6	76.4	0.3	24
1995	71.1	3	84.8	0.7	25.9
1995	83.7	6	91.9	1	34.1
1995	72.7	3	86.5	1	26.5
1995	83.9	0.8	96.1	1	32.3
1995	78.1	7	91.6	1	29.1
1995	78.8	4	87.2	0.5	31.9
1995	59.6	1	77.7	0.3	18.5
1995	66.5	1	89.5	0.8	19.3
1995	66.4	2	89.4	1	19.3
1995	65.1	0.4	81.8	0.4	21.7
1995	65.2	0.9	81.9	0.4	21.8
1995	69.4	0.4	91.3	0.6	21.2
1995	65.5	2	91.4	0.6	17.4

Partial dataset from (Johnston et al., 1997)